Emission of ^{3}He, ^{4}He and ^{6}He particles produced from the interaction of ^{12}C with ^{93}Nb at 400 MeV incident energy

Lufuno Julia Mudau

A thesis submitted in partial fulfilment of the requirements

for the degree of Magister Scientiae

in the Department of Physics,

University of the Western Cape

Supervisor: Prof. R. Lindsay

June 2005

KEYWORDS

- Projectile break-up
- Nucleon Coalescence
- Mean Field Interaction
- Incomplete Fusion
- Complete Fusion
- Compound Nucleus
- Inclusive Spectra
- Particle Identification (PID)
- Prescaled Singles
- Double Differential Cross Sections

Emission of ^{3}He, ^{4}He and ^{6}He particles produced from the interaction of ^{12}C with ^{93}Nb at 400 MeV incident energy

Lufuno Julia Mudau
*i*Themba LABS, P. O. Box 722,
Somerset West, 7129
e-mail:mudau@tlabs.ac.za

Abstract

The inclusive double differential cross sections of ^{3}He, ^{4}He, and ^{6}He particles produced from the interaction of ^{12}C with ^{93}Nb at 400 MeV incident energy were extracted from the prescaled singles spectra which were measured in conjunction with the correlation between ^{8}Be fragments and α particles. A further aim of this project was to test the detector efficiencies and energy calibrations by comparing the alpha and ^{8}Be prescaled singles data with existing inclusive cross sections of the same reaction. The absolute cross sections of ^{3}He and ^{6}He fragments have been extracted based on the absolute normalization of the alpha particle spectra. A study of the inclusive spectra of ^{3}He and ^{6}He suggest similar features to those seen in the alpha particle spectra. These features are described by the projectile break-up and nucleon coalescence mechanisms. A theoretical model which takes both these mechanisms into account was applied to describe ^{3}He and ^{6}He fragments. The model is able to reproduce reasonably well the inclusive energy spectra of the ^{3}He and ^{6}He fragments. These results are found to be consistent with previous studies of the emission of intermediate mass fragments.

U bveledzwa ha zwipida zwa ^{3}He, ^{4}He na ^{6}He kha vhutanganyi ha ^{12}C na ^{93}Nb kha maanda a 400 MeV.

Lufuno Julia Mudau
*i*Themba LABS, P. O. Box 722,
Somerset West, 7129
e-mail:mudau@tlabs.ac.za

Manweledzo

Dzi *differential cross sections* dzo katelaho kavhili dza zwipida zwa ^{3}He, ^{4}He na ^{6}He zwo bvaho kha vhutanganyi ha ^{12}C na ^{93}Nb kha maanda a 400 MeV dzo bviswa dzi tshibva kha zwi-*spectra* vhuthihi wo elwaho u thoma zwo kalwa hu tshi katelwa na u vhambedzwa ha ^{8}Be na zwipida zwa ^{4}He zwezwa vhonwa kathihi. Tshipikwa hafhu tsha iyi thandela ho vha hu u linga vhukoni ha *detector* na tshikalo tsha maanda nga u vhambedza zwidodombedzwa vhuthihi zwo kalwaho u thoma zwa ^{4}He na ^{8}Be, na dzi *cross sections* dzo katelaho dza vhutanganyi vhu fanaho. Dzi *cross sections* vhukuma dza zwipida zwa ^{3}He na ^{6}He dzo nulwa ro di tika nga u leludzwa vhukuma ha zwipida zwa ^{4}He. Zwi-*spectra* zwo katelaho zwa ^{3}He na ^{6}He zwo sumbedza maitele a vhutanganyi a fanaho na o vhonwaho kha zwi-*spectra* zwa zwipida zwa ^{4}He. Maitele aya ndi u khaukana hatsho poswaho na thanganyo ya dzi-*nucleons*. Tshifanyiso kholekhole tshi dzhielaho nzhele maitele aya tsho shumiswa u talusa zwipida zwa ^{3}He na ^{6}He. Tshifanyiso itshi tshi kona u vhusa nga ndila i pfadzaho zwi-*spectra* zwa maanda zwo katelaho zwa ^{3}He na ^{6}He. Mvelelo idzi dzi khou wanala dzi tshi andana na dza kha ngudo dzo fhiraho dza vhubvledzi ha zwipida zwa zwilime-kati.

DECLARATION

I declare that *Emission of ^{3}He, ^{4}He and ^{6}He particles produced from the interaction of ^{12}C with ^{93}Nb at 400 MeV incident energy* is my own work, that has not been submitted for any degree or examination at any other university, and that all the sources I have used or quoted have been indicated and acknowledged by completed references.

Full name.....Date..... Signed.....

ACKNOWLEDGEMENTS

- First, I would like to thank God who made it possible for my research to be conducted and completed in time.
- I would like to thank my University supervisor Prof. R. Lindsay, my co-supervisor Dr. S. V. Förtsch, for their invaluable supervision and encouragement that lead to the successful completion of my research project.
- I would also like to thank Dr. E .Z. Buthelezi for her support with the theoretical treatment of the code.
- I would also like to thank Drs. S. Connell, H. Fujita, R. Neveling, E-Sideras Haddad, F. D. Smit, and G. F. Steyn, for their many hours of data taking.
- I wish to express immense gratitude to my family for their love, sacrifice, dedication and encouragement through the tenure of my studies.

Contents

List of Figures

List of Tables

Chapter 1

Introduction

Initial studies in a series of experiments [Gad97], [Gad98] measured the excitation functions and recoil range distributions of especially near-target mass residues produced in the interaction of α-cluster-type light nuclei e.g ^{12}C and ^{16}O, with ^{103}Rh using the stacked-foil activation technique. These residues were identified by detecting characteristic γ-lines and by measuring their half-lifes. The activation technique was also advantageous in that it was possible to identify with absolute certainty a given residue. By measuring the excitation functions for production of a series of isotopes of decreasing mass and charge, one obtains information about the reaction mechanisms. In this reactions, one may assume that the mean field interaction (one body dissipation mechanism) leads to either fusion of the projectile with the target, or to the break-up of the projectile into a spectator fragment that flies away without further interactions with the target nucleus, and while the participant fragment fuses with the target nucleus. The data from these measurements suggest that the dominant contribution to these reactions is the complete and incomplete fusion of α-type projectile fragments.

The emission of a large number of alpha particles which were observed in

these previous studies [Gad97] with special emphasis on testing a theory which assumes that the primary interaction between the projectile and the target nucleus leads to the incomplete fusion of the projectile fragment with the target nucleus, prompted a set of inclusive measurements (summing up all contributions of the reaction processes in which the observed fragment is produced) of alpha particles produced in the interaction of ^{12}C with ^{93}Nb at 400 MeV incident energy. In these experiments, thin rhodium targets could not be used since they require a polymer backing. Since the reaction mechanisms should not depend on the mass of the target nucleus, a nearby mass and charge nucleus, ^{93}Nb, with self supporting foils was used.

In subsequent experiments, inclusive spectra of other α-like fragments such as ^{12}C and ^{8}Be fragments were also measured in ^{16}O and ^{12}C induced reactions on ^{93}Nb, respectively, at incident energies between 100 MeV and 400 MeV. These studies not only form a continuous test of the theory, but they also provide a way of experimentally determining the absolute values of the incomplete fusion cross sections and the excitation energy distributions of the nuclei produced after the incomplete fusion process. The spectra of fragments produced by a binary fragmentation process have a smaller average energy and a broader energy distribution than predicted by the Serber formalism [Ser47]. This suggested a possible initial state interaction between the projectile and the target nucleus or the final state interaction of the participant fragment with the target nucleus.

The study of the inclusive spectra of ^{8}Be fragments produced from the binary fragmentation of ^{12}C hypothesized that the observed break-up contribution to the measured ^{8}Be spectra could be reproduced by taking into account the dominance of the initial state interaction between the projectile and the target. The inclusive spectra of ^{7}Be and ^{9}Be fragments were measured to ac-

count for final state interactions between the outgoing ^{8}Be and the residual nucleus [Bec03]. However, contributions from such interactions were negligible and it was therefore concluded that the binary fragmentation of the projectile with a reduced energy as a consequence of the friction dissipative mechanism between the projectile and the target, prevails to be the dominant mechanism. Extensions of these investigations is the correlation of the ^{8}Be fragments and ^{4}He particles produced in the binary fragmentation of ^{12}C. The study of the ^{8}Be fragments is of importance since it is unlikely that once produced a ^{8}Be fragment will survive any final state interaction without loosing the correlation between its two constituent α-particles in a way in which it is detected and identified. Thus, one merely has to consider the final state interactions of the alpha particle in inelastic fragmentation (participant fragment interacts and even fuses with the target).

The present study which evolved from the α-^{8}Be correlation experiment and in which the spectra of ^{3}He, ^{4}He, and ^{6}He were measured, is a continuous test and extension of the theory to describe the energy spectra of ^{4}He particles and other intermediate mass fragments IMF's (fragments with atomic number $3 \leq Z \leq 14$).

This theory is described by the binary fragmentation as well as nucleon coalescence incorporated in a code developed at the University of Milan.

1.1 Reaction Mechanisms

1.1.1 Overview

Several reaction mechanisms are operative at intermediate energies. Predominant among these are, complete fusion, deep-inelastic collision, and quasi-

elastic collisions at energies below 10 MeV/n [Fuc94]. As the energy increases, i.e. above 10 MeV/n, the binary fragmentation of the projectile and nucleon-nucleon collisions becomes dominant. Heavy ion reactions induced by light ions such as ^{12}C and ^{16}O projectiles have led to the emission of intermediate mass fragments (IMFs) and particles at intermediate energies varying from a few MeV/n up to several hundred of MeV/n. Studies by McVoy et al. [McV80] have shown that the projectile fragmentation spectra are dominated by a quasi elastic peak of particles with energies corresponding to the beam velocity. Martinez et.al [Mar85] considered cases in which the heavy fragment is produced in a binary fragmentation and subsequently undergoes a dissipative interaction with the target nucleus, while Möhring et al. [Möh91] considered cases in which a frictional force acts between the projectile and the target before the break-up of the projectile. The inclusive spectra of ^{15}N and ^{12}C resulting from bombardment of ^{208}Pb by ^{16}O in the energy range 140-315 MeV have shown strength at forward angles. This was in approximate agreement with data of Gelbke et al. [Gel77], [Gel78]. In these studies the spectra for lighter projectile fragments are peaked at lower emission energies and extended to the exit-channel Coulomb barrier, indicating a contribution from deep inelastic events.

1.1.2 Fragmentation

The projectile break-up also known as far break-up as described in the perturbative Serber approximation [Ser47], [McV80], and [Gad99] has a maximum at the energy corresponding to the beam energy and a peak related to the momentum distribution of the observed fragment within the projectile. This is assumed to be a peripheral direct reaction by which the projectile breaks-up into two fragments which may be emitted without further interactions with the target nucleus(quasi elastic fragmentation), or the stable fragments

may excite and even fuse with the target nucleus (inelastic fragmentation).

1.1.3 Thermalization and Nucleon Coalescence

When two heavy-ions fuse they form a composite nuclear system that is far from statistical equilibrium since a large fraction of its energy is in the form of an orderly translational motion of the nucleons of the projectile and the target nucleus [Hod97]. This orderly collective motion transforms into chaotic motion through the cascade of nucleon-nucleon interactions during the thermalization of the composite nucleus. Once the process reaches thermal equilibrium a nucleon or group of nucleons with a considerable energy higher than their equilibrium thermal energy may be emitted into the continuum.

The spectra of fragments produced in the transfer of a nucleon or group of nucleons from the projectile to the target have a lower energy component and a width that increases with increasing emission angle. This feature of the spectra is associated with the coalescence of nucleons during the cascade of nucleon-nucleon interactions by which the intermediate excited nuclei which are produced during the complete fusion of the projectile with the target nucleus or partial fusion of the projectile fragments with the target nucleus reach a state of statistical equilibrium. The coalescence model was first introduced in heavy-ion reactions to account for the spectra of light composite ejectiles [Awe81], [Awe82]. The model was later improved by [Cer92], [Cav96] to predict the emission of IMFs with energies about equal to the Coulomb barrier. Within this model the emission of IMFs was evaluated based on the assumption that an IMF, whose momentum falls into the sphere of radius $p_{c,F}$ in momentum space, may be produced by a coalescence mechanism during the intranuclear interaction cascade by which the kinetic energy of the projectile

transforms into random thermal energy.

1.1.4 Complete Fusion

This process involves the full momentum transfer from the projectile to the target nucleus leading to the formation of an excited compound nucleus.

1.1.5 Incomplete Fusion

This is described as a process in which both fragments come out (participant and spectator) after interaction, but one of them having interacted with the target nucleus.

1.1.6 Deep-Inelastic Collision

Heavy-ion reactions at energies below 10 MeV/n are dominated by deep-inelastic collisions [Fuc94]. In these type of collisions the nuclei come into contact with one another and a portion of the kinetic energy is converted into Coulomb potential energy. This implies that they may be moving slowly enough so that during the period of contact as they pass each other, there is enough time for a large amount of the remaining kinetic energy to be converted into internal excitation. This energy dissipation occurs via nucleon-nucleon interaction and mass exchange through the region of contact where a neck of nuclear matter may form as the two nuclei stick together and begin to rotate as a single unit. Since the angular momentum is too high for fusion to occur and, a short time later, the fragments separate. They then acquire extra energy from their mutual Coulomb potential energy as they repel each other. During contact, nucleon transfer occurs in both directions and the masses and charges of the final products may not be very different from those of the initial reactants. However, contact time does not last long

enough for a complete rotation of the combination to take place and the angular distribution is peaked in the forward direction.
The presence of these collisions in heavy-ion reactions are dominated by mean fields in this energy region and the ions still maintain their binary character. As the energy of the projectile increases, these collisions can no longer hold and thus other reaction mechanisms predominate.

1.1.7 Evaporation

Reactions that proceed from the initial channel c through the compound nucleus to the final channel c'can be used to predict the weak dependence of the energy average cross-sections [Hod97]. The compound nucleus may be created in states of different angular momentum J, then the hypothesis of the independence of formation and decay of the compound nucleus gives for the cross-section

$$\sigma_{cc'} \approx \sigma_{CN}(c)\frac{\Gamma_{c'}}{\Gamma} \tag{1.1}$$

where, σ_{CN} is the cross section for formation of the compound nucleus, $\Gamma_{c'}$ is the energy-averaged width for the decay of the compound nucleus in channel c', and Γ is the energy-averaged total width of the compound nucleus.
The theory provides a simple way of estimating the energy variation at low incident energies of the cross sections of all available final channels in a particular reaction. The estimation of the energy variation is based on the nuclear level densities and compound nucleus formation cross section. It does not consider the conservation of angular momentum nor does it give evidence for the angular distributions of emitted particles. Because of its inadequacy in producing the angular distributions of emitted particles, a Hauser-Feshbach [Hod97] theory was introduced. The theory takes into ac-

count the formation of the compound nucleus in states of different angular momentum J and parity.
The theory has been tested on nucleon-induced reactions and on reactions induced by α particles. However, studies induced by light ions such as ^{12}C and ^{16}O have shown a tail which extends to lower emission energies (as compared with the break-up process at higher emission energies) which could be explained in terms of the evaporation process.

1.1.8 Pre-equilibrium emission

This process is described as the emission of fast particles prior to equilibration of the compound nucleus. Pre-equilibrium emission and intranuclear interaction cascade are described within the framework of the Boltzmann Master approach [Cav01].

1.2 Milano Model

A more general theory that has been developed at the University of Milan to explain the observed spectra of emitted particles and IMF's [Bec03], [Gad01] has in this study also been applied to the emission of ^{3}He and ^{6}He fragments. It appears that these fragments are produced by same mechanisms as ^{4}He, as evidence by previous ^{4}He spectra [Gad99], which were produced in the interaction of ^{12}C with ^{93}Nb and ^{59}Co at 400 MeV incident energy.

The model considers reaction mechanisms such as the complete fusion, incomplete fusion, single nucleon transfer as well as inelastic scattering reactions, to evaluate the excitation functions, angular distributions of particles and intermediate mass fragments (IMFs). It has been extended in the present study to also evaluate the emission of ^{3}He and ^{6}He particles by considering

the projectile break-up and nucleon coalescence mechanisms. In these code, the projectile break-up is evaluated under the hypothesis of the Serber approximation [Ser47] and the local plane wave approximation [McV80], while the nucleon coalescence is evaluated within the framework of the Boltzmann Master equation theory (BME) [Cav96], [Cav97], [Cav98], [Cav01]. In the previous studies [Bec03], [Gad01], the spectra of break-up fragments were produced with the broadening and softening of the distribution width which could be explained by introducing the energy loss by the projectile in an initial state interaction with the target nucleus.

In the present study, the dominance of the initial state interaction of the projectile was also considered for the analyses of the ^{3}He and ^{6}He spectra produced in the interaction of ^{12}C with ^{93}Nb at 400 MeV incident energy. Mass separation was possible in this case particularly because of the absence of ^{5}He in the particle identification spectrum.

1.3 Motivation of Study

The original motivation from which this study followed, was to ascertain the importance of quasi-elastic fragmentation and inelastic fragmentation from an experiment which was designed to measure the correlation between ^{8}Be fragments and ^{4}He particles produced in the interaction of ^{12}C with ^{93}Nb at 400 MeV incident energy. The objectives of the data analysis were twofold. Firstly, in order to test the energy calibrations and detector efficiencies the prescaled singles of ^{4}He particles and ^{8}Be fragments were overlaid onto the existing inclusive cross sections [Gad99], [Gad01]. Secondly, to extract the inclusive double differential cross sections from the prescaled singles of ^{3}He

and ^{6}He from by using the same normalization obtained from the ^{4}He data.

The mono-isotopic nature of the ^{3}He and ^{6}He spectra, due to the absence of ^{5}He in the particle identification spectrum, allows for a thorough test of the proposed reaction mechanisms. This study therefore aims at investigating to what extent projectile break-up as well as nucleon coalescence can also reproduce the inclusive double differential cross sections of ^{3}He and ^{6}He.

The experimental set-up as well as the electronics used for the data acquisition are described in chapter 2. The procedure of the data taking as well as the analysis of the data are described in chapter 3. In chapter 4 the theoretical description of various reaction mechanisms that were incorporated into the code are described. In chapter 5 the experimental and theoretical double differential cross sections of ^{3}He and ^{6}He particles are presented. The summary and conclusions are described in chapter 6, while the parameters used in the calculations are described in the appendix.

Chapter 2

Experiment

2.1 Overview

This experiment had two aims. The first was to measure the coincidence events of the ^{8}Be fragments and ^{4}He particles produced in the interaction of ^{12}C with ^{93}Nb at 400 MeV incident energy. Of specific interest were the prescaled singles events of ^{3}He, ^{4}He, ^{6}He, and ^{8}Be. The prescaled singles events (singles events prescaled by a factor 20 to reduce pile-up with the coincidence data) were accumulated with a prescaling factor which accepted 5 % of the singles events in each detector telescope. An event is described as an alpha particle or a ^{8}Be fragment that strikes a detector and singles events are accumulated when there is a coincidence between $\Delta E1$ and $\Delta E2$ or between $\Delta E2$ and the E detector in telescopes 1 and 2. The amplifier gains and thresholds were selected to optimize the detection of the ^{3}He, ^{4}He, ^{6}He, and ^{8}Be, thereby precluding complete information of other lighter ejectiles. Apart from the coincidence events, prescaled singles and pulser events were also recorded. The second aim of this project was to test the detector efficiencies as well as on the measurement of the prescaled singles events. Both the experimental set-up as well as the electronics used to measure and

process these events will be described in this chapter.

2.2 Detectors

2.2.1 Silicon surface barrier detectors

Charge sensitive silicon surface barrier (SSB) ΔE detectors were used as transmission detectors which measure the energy lost by a charged particle passing through it. Some of the characteristics of these detectors include:

- the means to detect bound charged particles due to low intrinsic conductivity
- ability to operate at room temperature without excessive leakage current
- thin dead layers
- energy loss distribution function
- surface area of the SSB

2.2.2 Silicon Strip Detector (SSD)

Since the ^{8}Be nuclei cannot be detected as single entities, the two correlated alpha particles constituting a ^{8}Be need to be detected in coincidence. In order to process the ΔE information of each alpha particle, a detector equipped with individual strip readouts needs to be provided for each strip. The silicon strip detector was found to meet the requirements for such purposes. With this detector the angular and energy information of the two correlated alpha particles constituting a ^{8}Be can be used to reconstruct the kinematics of the decay event.

2.2.3 Design of the Silicon Strip Detector

An important aspect to consider in the design of the Silicon strip detector is maximizing the effective solid angle for the detection of the ^{8}Be. The following practical considerations should be taken into account when designing the ^{8}Be telescope

- charge sharing and cross-talk between the strips
- the need to instrument signals for all strips

The effective solid angle for the ^{8}Be detection depends on the geometry of the strip detector, on the distance of the detector from the target, and on the excitation energy of the ^{8}Be [Woz92]. The effective solid angle of this telescope is obtained by using the Monte Carlo program, described in section 3.5.

2.2.4 NaI detector

A NaI E detector is a scintillation type of detector which makes use of the fact that certain materials when interacting with nuclear radiation emit a flash of light. The stopping E detector has a NaI crystal of 76.2 mm in diameter and 50.8 mm in thickness. A Havar entrance window of 50.8 mm in diameter and 7 μm in thickness slightly degrades the energy of the particles before entering the NaI detector. It also protects the NaI crystal against moisture. The basic characteristic of this detector is its response to various charged particles which is essentially the efficiency for converting ionization energy to photons. The response is described by the light output which is different for different charged particles (see energy calibrations of telescope 1).

2.3 Experimental Procedure

2.3.1 Beam Energy

The separated sector cyclotron (SSC) at iThemba LABS can accelerate carbon ions up to a maximum energy of 35 MeV/nucleon. The development of a 400 MeV ^{12}C beam starts with an external electron cyclotron resonance (ECR) ion source which produces ions and accelerates them to a few tens of keV. The ions are then further accelerated to a few MeV by means of a solid pole cyclotron (SPC2) after which the ions are accelerated in the SSC. After extraction from the SSC the beam is transported along beam lines to the A-line vault where high energy scattering experiments are performed (see Fig.2.1). A beam intensity of less than 5 electrical nA was delivered to the experiment.

2.3.2 Scattering Chamber

The 1.5 m diameter scattering chamber located in the A-line vault is equipped with two rotatable arms. The scattering chamber has various ports. One is connected to the incoming beam-line and another to the beam stop. Another port is used for a closed circuit television camera to view the scintillation of a ruby target produced by the beam spot while focusing the beam. The other ports are equipped with cable feed throughs which are used to feed cables to connect the output of the preamplifiers mounted inside the chamber. In order to reach a pressure of 10^{-5} mbar the chamber was pumped down in the following three stages: First the valve between the scattering chamber and the rotary and turbo-molecular pump was opened. A pressure of l mbar was attained with the rotary pump after which the turbo-molecular pump was started. At a pressure of about to 10^{-3} mbar the valve to the cryo-pump was opened. This pump has a cold surface at 12 K which traps any remaining

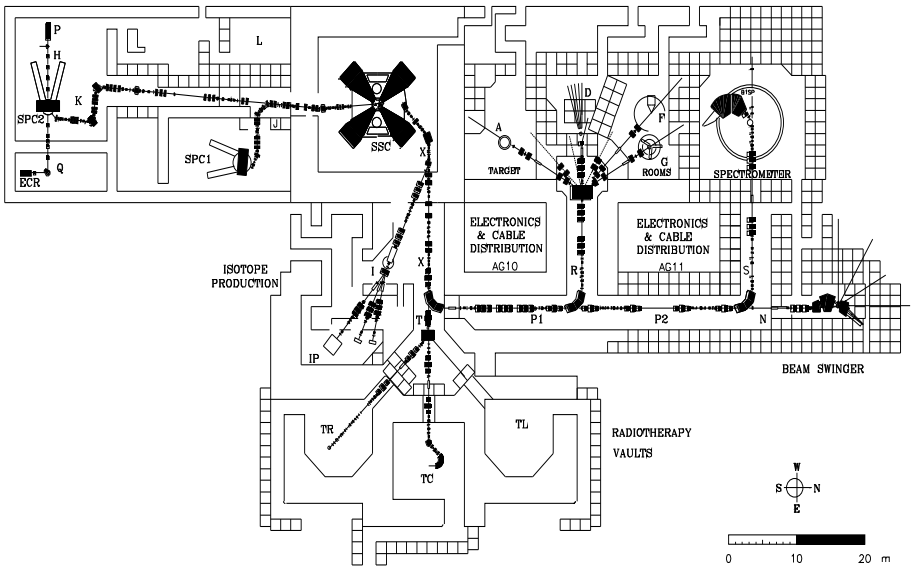

Figure 2.1: Layout of the iThemba LABS cyclotron facility .

molecules inside the chamber. At a pressure of approximately 10^{-4} mbar the detectors were biased. The valves to the beam line and beam stop were then opened so that the beam could be delivered along the A-line into the scattering chamber. A schematic diagram of the detectors in the scattering chamber is shown in Fig.2.2.

2.3.3 Target

A ^{93}Nb target of thickness 1.05 mg/cm^2, was mounted in an aluminium frame of 25 mm diameter. The frame was mounted onto an aluminium ladder that fits into the target drive mechanism situated at the center of the scattering chamber. The thickness of the target was confirmed by measuring

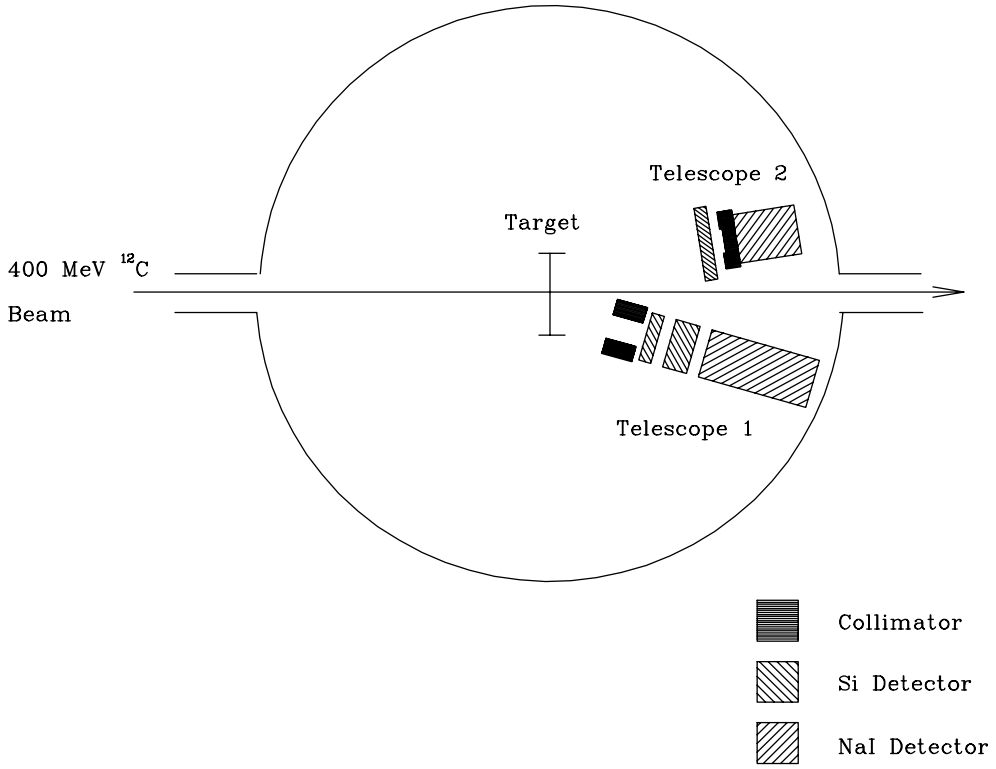

Figure 2.2: Schematic diagram of detector telescopes inside the scattering chamber.

the energy loss suffered by alpha particles from a ^{228}Th source in the target. A scintillating ruby target with a hole of 3 mm diameter was used to align and monitor the beam with a spot of less than 3 mm diameter. An empty frame target was positioned to the beam spot to check the beam halo. Beam halo is inherently produced in all charged particle beams and it is monitored by comparing the count rates, produced when an empty frame target is placed in the beam path, to the counts with a target in place.

2.3.4 Detector Telescopes

Two detector telescopes were mounted on rotatable arms inside the 1.5 m diameter scattering chamber located in the A-line vault (see Fig.2.2). Telescope 1 used two ΔE silicon surface barrier detectors and a stopping NaI E detector to measure ^{3}He, ^{4}He, and ^{6}He. A resonant particle spectrometer consisting of a position sensitive SSD with 16 strips as the ΔE detector followed by a stopping NaI E detector, was used to measure the two correlated alpha particles constituting a ^{8}Be in telescope 2.

Telescope 1

Provision was made to include low energy alpha particles by using two ΔE detectors of different thicknesses. The first detector element, referred to as the $\Delta E1$ detector, had a thickness of 27.6 μm followed by a $\Delta E2$ detector of thickness 522 μm. A brass collimator of thickness 48.33 mm and a diameter of 13.8 mm was placed in front of the ΔE detectors. The distance from the center of the target to the exit of the collimator was 276.0 mm. The data with this telescope were taken in an angular range from 16° to 30° in 2° steps. The solid angle of this telescope was calculated from the equation

$$\Delta\Omega = \frac{\pi r^2}{R^2} \tag{2.1}$$

where,

$r \equiv$ *radius of the collimator*

$R \equiv$ *distance from the center of the target to the exit of the collimator*

The solid angle subtended by telescope 1 was 2.000 ± 0.032 msr.

Telescope 2

The SSD used has 16 vertical anode and 16 horizontal cathode strips with an active area of 50 mm × 50 mm. The strips are 3 mm wide and have an inter-

strip gap of about 0.1 mm. The thickness of the SSD used was 284 μm while the distance from the center of the target to the front of the detector was 450.81 mm. A brass collimator with a 63.5 mm aperture and 7 mm thickness placed between the SSD and the NaI detector prevented the alpha particles from being degraded by the window flanges upon entering the NaI crystal. Data with this telescope were taken at a fixed angle of 9° with respect to the beam axis throughout the measurements.

2.4 Electronics

The electronic set-up which was used to process the signals of coincidence events, prescaled singles events, and pulser events will be described in this section.

2.4.1 Detector Signals and pre-amplifiers

Since the signals arising from the detectors are small, all the pre-amplifiers were mounted inside the scattering chamber close to the detectors. In the case of telescope 2, the 8-channel preamplifier modules were mounted on top of the brass cage (which surrounds the detector in order to reduce the electronic noise) close to the SSD, while for the NaI E detectors, scintillation type pre-amplifiers were used. The types of signals dealt with in this experiment include the linear and logic signals.

2.4.2 Linear signals

These signals give information on the energy of the particle detected. The linear signals from the pre-amplifiers in telescope 1 were transmitted through the standard BNC 93 Ω coaxial cables to the amplifiers in the data room. The energy signals in telescope 2 were processed from 16-channel preamplifier

modules to the 16-channel amplifier modules. Signals from events of interest were selected by logical requirements. These logic signals were then used to generate the gates for the linear gate and stretcher (LGS) modules which gated the linear signals to the analog-to-digital converter (ADC) modules. The gate signals were inhibited by a computer busy signal. The electronic diagram used to process the linear signals is shown in Fig.2.3. The NIM modules used to process the linear signals are listed in Table 2.1.

Table 2.1: NIM modules used to process the linear signals

Module	*Type*
Charge Sensitive Preamplifier	ORTEC 142
Light-Sensitive Preamplifier	ORTEC 113
8-Channel Preamplifier	IN-HOUSE
Spectroscopy Amplifier	CANBERRA 2021
16-Channel Amplifier	CAEN N568B
Linear gate and stretcher (LGS)	ORTEC 542
Analog-to-digital converter (ADC)	CANBERRA 8077
8-channel Silena ADC	SILENA ADC 4418/V

2.4.3 Logic signals

Fast timing signals have a fixed shape and simply indicates the presence o absence of a signal. The logic signals of telescope 1 were fed from each detector preamp into the timing filter amplifier (TFA) each followed by a constant fraction discriminator (CFD). A 4-fold logic unit (4FLU) module was used to perform the AND and OR operations between the ΔE and E detectors. The coincident firing of detectors$\Delta E1$, and $\Delta E2$, in anti-coincidence with the NaI detector, indicate that a low-energy α has been detected. This is denoted by $A \cap B \cap \bar{C}$, where A denotes a signal from the $\Delta E1$ detector, B a signal

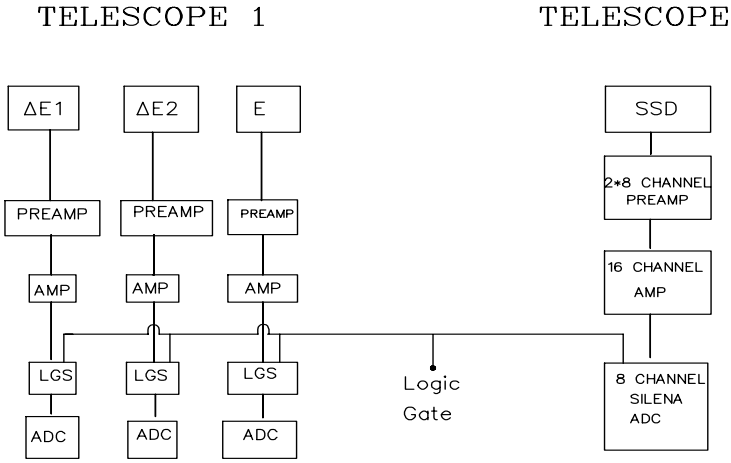

Figure 2.3: Electronic diagram used to process linear signals in telescopes 1 and 2.

from $\Delta E2$ detector, and $\bar{C}$ means no signal from the E detector. The high energy alpha particles resulted in a coincidence between the $\Delta E2$ detector and the E detector. This is denoted by $B \cap C$. A 4FLU module selected the coincidences for the low and high energy alpha particles in telescope 1 with a coincidence level of 2. Events accumulated as prescaled singles events, i.e. after every 20^{th} event was accepted, were generated by the gate and delay generator (GDG), timer and level adapter.

The ^{8}Be prescaled singles events from telescope 2 were processed in a similar way as in telescope 1. The logic signals of telescope 2 were fed from the 8-channel preamplifier modules to the coincidence unit. A 4FLU module selected the overall coincidences between telescope 1 and telescope 2. Gate signals were generated by a GDG after identifying the events either as a low-energy or a high energy-alpha event. The event trigger was generated by the CAMAC event trigger module. For every event trigger this module also raised a computer busy signal. An event trigger was raised for the follow-

ing types of events: prescaled singles events, coincidence and pulser events. A diagram of the electronics used to process the logic signals is shown in Fig.2.4. The NIM modules that were used to process the logic signals are listed in Table 2.2.

Table 2.2: NIM modules used to process the logic signals

Module	*Type*
Timing filter amplifier (TFA)	ORTEC 474
Constant fraction discriminator (CFD)	ORTEC 934
4-fold logic unit (4FLU)	LECROY 365AL
Discriminator (DISC)	LECROY 821
8-CH Autowalk Discriminator (DISC)	CAEN N415A
Logic fan-in-out (FAN)	LECROY 428F
Timer	ORTEC 719
Coincidence unit	IN-HOUSE 32 CH

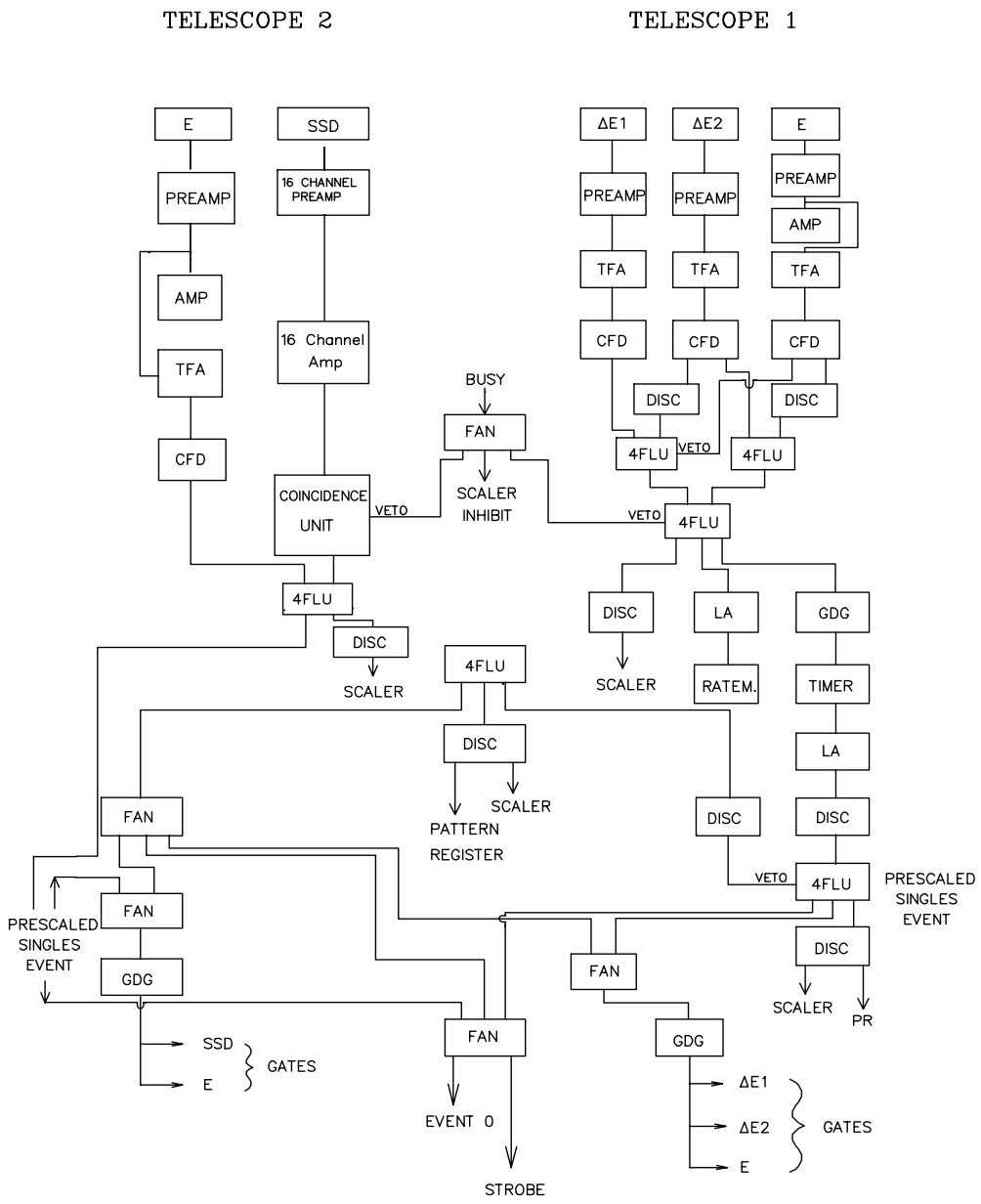

Figure 2.4: Electronics diagram used to process logic signals from telescopes 1 and 2.

2.4.4 Current Integrator

The ^{12}C beam measured at the beam stop components was fed to the Brookhaven Instruments current integrator (BIC 1000C) module. This module allows selection of the current integrator range which determines the number of pulses output for every unit of accumulated charge. It also provides digital output pulses with a width of 5 μs.

2.4.5 Pulsers

Every detector element was provided with a pulser which was triggered at a rate proportional to the beam current. Every 20^{th} event of the current integrator signal triggered the tail pulse generator which sent signals to the test input of the pre-amplifiers. The purpose of the pulsers was to determine the electronic dead time and to monitor gain drifts in the photomultiplier tube of the NaI detector. The ratio of the pulser events from the ADC to the inhibited pulser from CAMAC scaler module gives an estimate of the electronic dead-time.

2.4.6 Event trigger

Events of interest were accepted in an event trigger unit module which enters the computer via a CAMAC module. This resulted in the generation of the computer busy signal. These events were identified in the bit pattern register as coincidence events, prescaled singles events and pulser events.

2.4.7 Computer busy

The computer busy signal was generated for every event accepted by the CAMAC event trigger module. These signals were fanned out in order to veto

the combined output of telescope 1 and the combined output of telescope 2 and to also inhibit the scalers.

2.4.8 Clock

A continuously running timer, was linked to the timing single channel analyzer (TSCA) and served as an electronic clock. The clock was fed to both an uninhibited and inhibited scaler. The difference between the two scaler readings gives an indication of the computer dead time.

2.4.9 Pattern register

The prescaled singles events, coincidence and pulser events generated were sent to the pattern register module. The pattern register was read for every event accepted. The strobe signal which is a delayed event trigger initiates the readout of the pattern register after the arrival of these events.

2.4.10 Scalers

Events acquired during the logical requirement 1 resulted in two sets of scalers which were counted by the two 12-fold Lecroy scalers. One set of these scalers was inhibited by the computer busy signal. Both scalers counted the total number of events in each detector telescope, total of accumulated charge as well as the pulser events.

Chapter 3

Data Analysis

3.1 Introduction

As an initial part of the data analysis, a test of the detector efficiencies and energy calibrations was performed by overlaying the current prescaled singles data onto the existing singles data sets. After confirming the energy calibrations and the detector efficiencies, a further step was taken to extract the double differential cross sections of the fragments of ^{3}He, ^{4}He, ^{6}He, and ^{8}Be from the prescaled singles data set. In this chapter, the experimental analysis of these fragments is described.

3.2 Data Handling

3.2.1 Data acquisition programs

The software package XSYS which operates on the VAX system was used for the data acquisition as well as for the event-by-event data replay. The online data acquisition was initiated through the following three stages:

- run XSYS

- load the VME files.
- load COM and EVAL files

The VME code build the event stream from information provided by the CAMAC interfaces of the ADC, Scaler, Bit Pattern Register and Event trigger modules and then feeds the data to the computer system for the data acquisition. The subprocess XSORT which uses the EVAL and COM file initiated the data sorting process. The COM file defines the data areas for various histograms to be stored and defines data areas for the 1-dimensional and 2-dimensional gates. The EVAL file unpacks every event and increments the spectra according to the event type.

3.2.2 Online Data Taking

The data taking was initiated by first aligning the beam spot on the ruby target. After the beam spot was properly aligned on the target the beam halo was monitored by comparing the count rates produced by the empty frame target and by the ^{93}Nb target. A background rate of less than 10 % was accepted. After the alignment and background check, the beam impinged onto the ^{93}Nb target. Data were collected in two hour runs and the experiment was run over three weekends including one weekend of tuning the electronics. The data for the ^{93}Nb target were collected over the remaining weekends at eight different emission angles.

3.2.3 Data Replay

The COM and EVAL files used for the data acquisition were extended for the data analysis defining additional data areas for the mass function gates and also for the energy spectra to be incremented in EVAL. The extended and existing COM and EVAL files were used during data replay.

3.3 Energy Calibrations

3.3.1 Telescope 1

The silicon detectors, herein referred to as $\Delta E1$ and $\Delta E2$, of telescope 1 were calibrated inside the scattering chamber by placing a ^{228}Th source in the opening of the collimator.

$\Delta E1$ detector

This Si detector of a thickness of 27.6 μm was calibrated by covering the exit of the brass collimator with an aluminium foil of thickness 25.4 μm. The aluminium foil was used to degrade the maximum alpha energy from a ^{228}Th source from 8.784 MeV to 5.338 MeV. The 5.338 MeV peak corresponded to channel 904.0. In the case of the alpha particles, this detector introduced an energy threshold of 8 MeV and a dead layer (window through which a portion of the particle energy will be degraded before reaching the active region of the detector)at about 36 MeV. As with ^{3}He and ^{6}He the threshold (low-energy cutoff for PID)was 32 MeV and 42 MeV, respectively.

$\Delta E2$ detector

In the case of the 522 μm $\Delta E2$ detector the full alpha energy spectrum as shown in Fig. 3.1 was observed. The channel numbers corresponding to the alpha particle energies from a ^{228}Th source were thus identified. The resulting linear energy calibration fit is shown in Fig. 3.2. The maximum energy that an α particle can deposit in $\Delta E1$ and $\Delta E2$ is 26 MeV. The energy resolution of this detector is 56 keV.
The calibration parameters for the slopes and offset of the ΔE detectors in telescope 1 are summarized in Table 3.1.

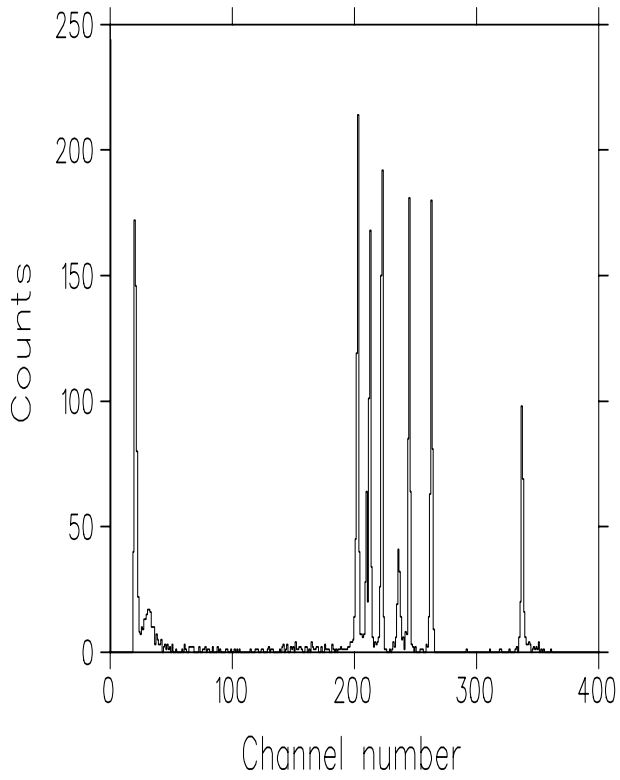

Figure 3.1: Energy spectrum for the alpha particles from the ^{228}Th source as measured with the 522 μm Si detector.

NaI *E* detector

The calibration parameters of the NaI detector were taken from previous measurements [Gad99],[Gad01] in which a 200 MeV alpha beam, was used to calibrate the detector. The calibration was based on the elastic scattering of alpha particles off the target. For consistency check, the double differential cross sections obtained from the current study are overlaid onto the existing singles data set [Gad99] (see Fig.3.3). As shown in the figures the results were found to be satisfactory at all emission angles studied.

The energy calibration of the E detector was adjusted separately for ^{6}He

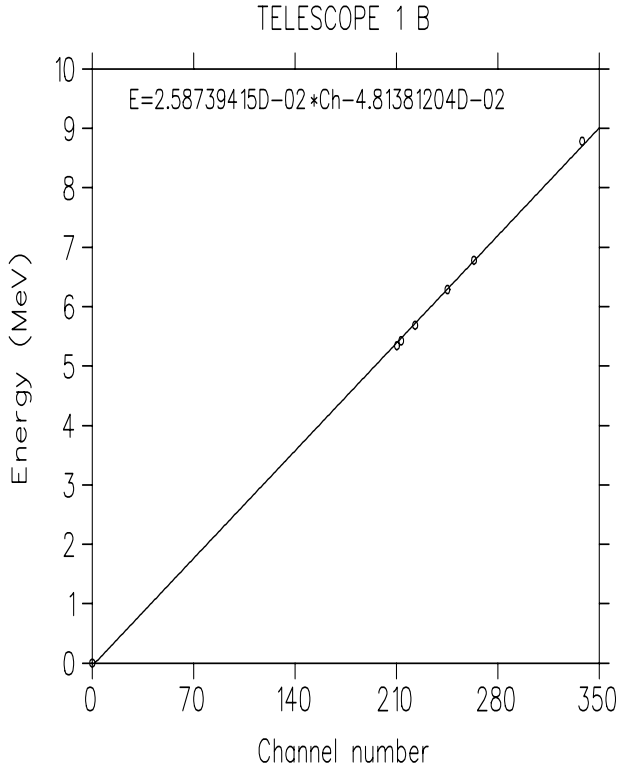

Figure 3.2: Energy calibration fit of the alpha particles in element B as shown in figure 3.1. Also shown are the corresponding calibration parameters for the slope and offset.

fragments and remained the same for ^{3}He and ^{4}He. This followed from the light output of various ions in NaI predicted by Michaelin et al., [Mic94]. This model is based on the assumption that the light produced by energetic ions in the scintillator material is related to the distribution of energy deposited by the secondary electrons produced along the ion track. The light output of the fragments studied was predicted using the theory described above. For ^{4}He and ^{3}He the light output response within the NaI detector remained the same, i.e the calibration parameter of the NaI detector was the same for ^{3}He and ^{4}He fragments. In the case of the ^{6}He fragments, the

Table 3.1: Calibration parameters of the ΔE detectors in telescope 1.

Detector	*slope*	*offset*
$\Delta E1$	0.005971	0.00
$\Delta E2$	0.025875	-0.048138

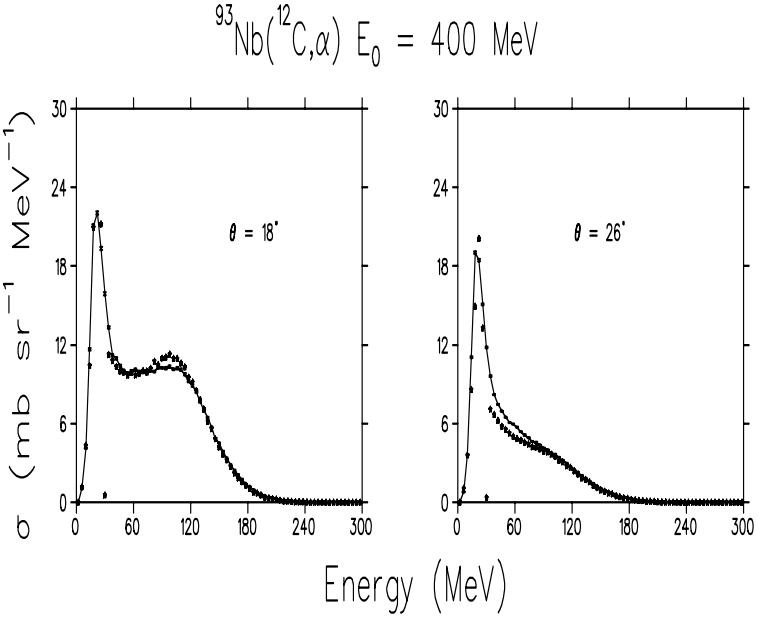

Figure 3.3: Double differential cross section spectra of ^{4}He particles emitted in the interaction of ^{12}C with ^{93}Nb at 400 MeV incident energy. The results are shown for telescope 1 at two emission angles. The diamonds represent the current results while the curves represent results from a previous measurement [Gad99].

light output was adjusted by 7 %. The calibration parameters of the NaI E detector are summarized in Table 3.2.

Table 3.2: Calibration parameters of the NaI E detector in telescope 1

Fragment	*Slope*
^{3}He	0.265
^{4}He	0.265
^{6}He	0.284

3.3.2 Telescope 2

In order to calibrate the SSD, ΔE-E particle identification (PID) spectra were generated during short runs with the coincidence level of the 4-Fold logic unit module of the SSD set to 1. This selected coincidences between any single vertical strip and the NaI E detector. The calibration of the SSD was based on the alpha particle spectra. Gates were set around the alpha loci in these PID spectra for purposes of offline calibrations of the SSD.

Since telescope 2 was at an emission angle of 9°, the elastic ^{12}C cross section was used to calibrate the NaI detector by determining the centroids of the elastic scattered ^{12}C peak at each weekend. The slope calibration parameter for this detector was 0.394.

Every silicon strip of the SSD (which had a thickness of 284 μm) was calibrated individually by overlaying the particle identification spectra on the energy loss calculations of the alpha particles in the ΔE and E detectors. The calibration parameters of telescope 2 obtained by fitting the energy loss curve onto the ^{4}He locus was 0.00489 for silicon strips 2 to 15. The energy loss calculations were obtained using the computer program ELOSS [Jip84]. An example of the calibration of the strip detector in coincidence with the NaI E detector is shown in Fig.3.4. A comparison of the ^{8}Be energy spectra between the current prescaled singles measurements and the existing singles

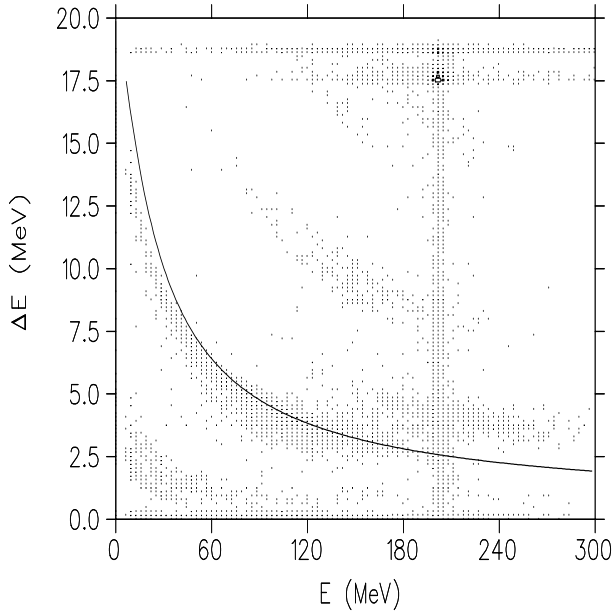

Figure 3.4: Calibration of the strip detector of telescope 2 based on single alpha particles when there was a coincidence between a single vertical strip and the NaI E detector. The curve represent the energy loss results fitted onto the ^{4}He locus.

measurement [Gad01] is shown in Fig.3.5 for an emission angle of 9°. This comparison confirms the detector calibrations and efficiencies of telescope 2.

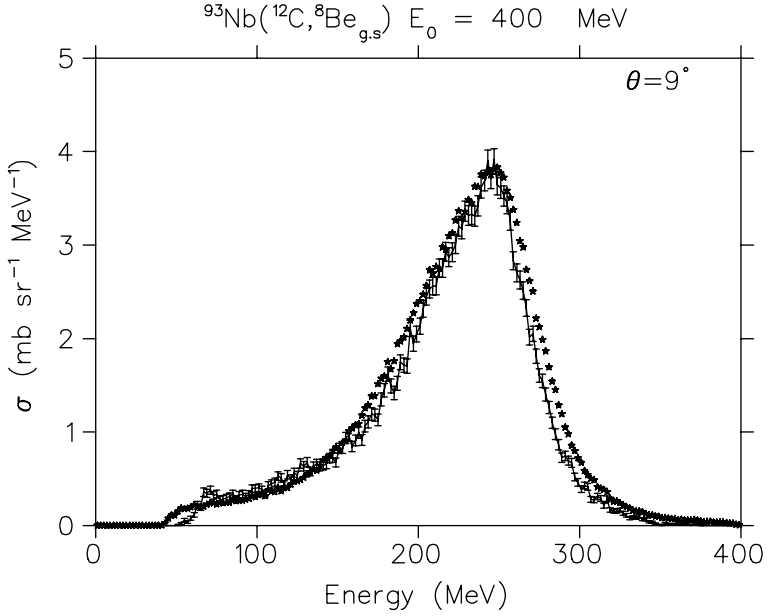

Figure 3.5: Double differential cross section spectrum of the ^{8}Be fragments emitted in the interaction of ^{12}C with ^{93}Nb at 400 MeV at an emission angle of 9°. The stars represent the current result while the curve represents the result from a previous measurement [Gad01].The error bars show the statistical error.

3.4 Particle Identification (PID)

The first step in the reduction of the data, i.e once the detectors had been effectively calibrated, was to identify the charged particles. The standard ΔE-E particle identification technique (PID) was employed to do charged particle identification of various charged particles in the range of $1 \leq Z \leq 4$.

3.4.1 Telescope 1

In the PID spectrum of element A against element B the fragments of ^{3}He and ^{6}He could not be clearly distinguished from the alpha particles (see Fig. 3.6).

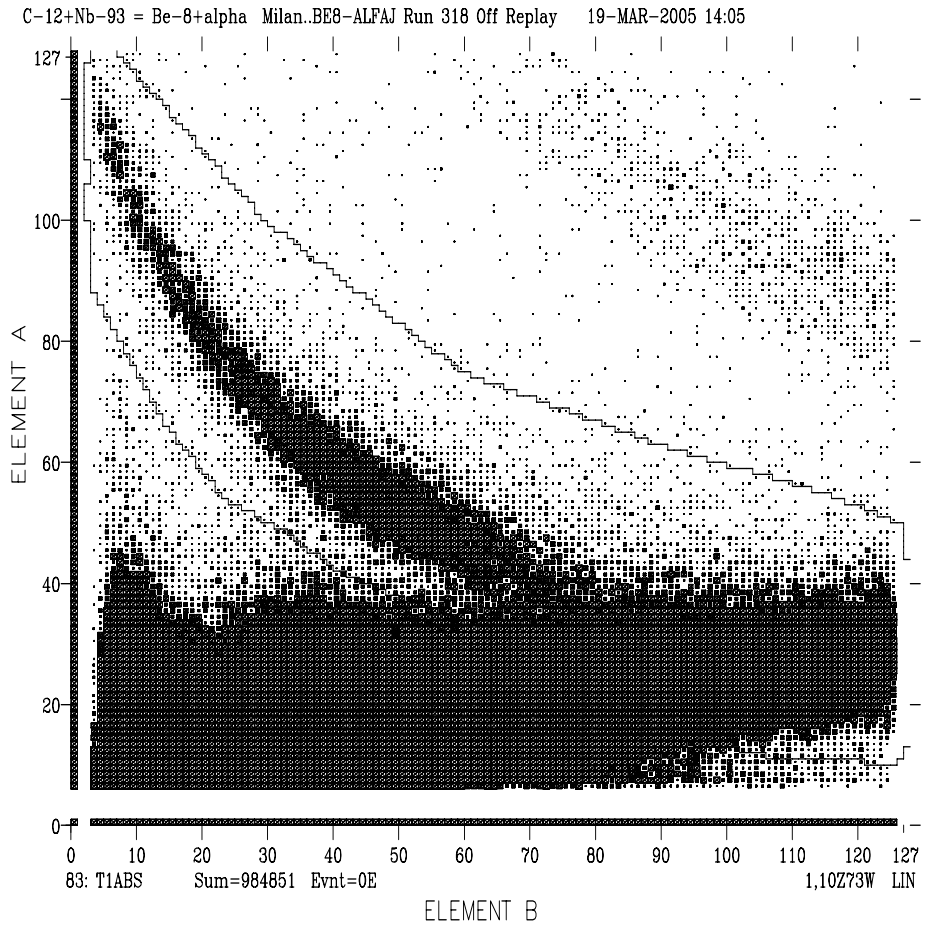

Figure 3.6: Particle identification spectrum of element A versus element B with a gate on the Z = 2 locus.

Thus a 2-dimensional gate was set around the Z = 2 locus. Because the mass resolution in element A was poor, it was necessary to calculate the energy using ELOSS of ^{3}He and ^{6}He. The calculated energy loss of ^{3}He and ^{6}He in element A were added to the measured energies deposited in B and C giving the total energy spectrum of each fragment. In the PID of element B against element C the separation between ^{3}He and ^{4}He is rather small (see Fig. 3.7) hence a 2-dimensional gate was set around the Z = 2 loci in order to

include events that fall within this gate. As a result, a mass function (given

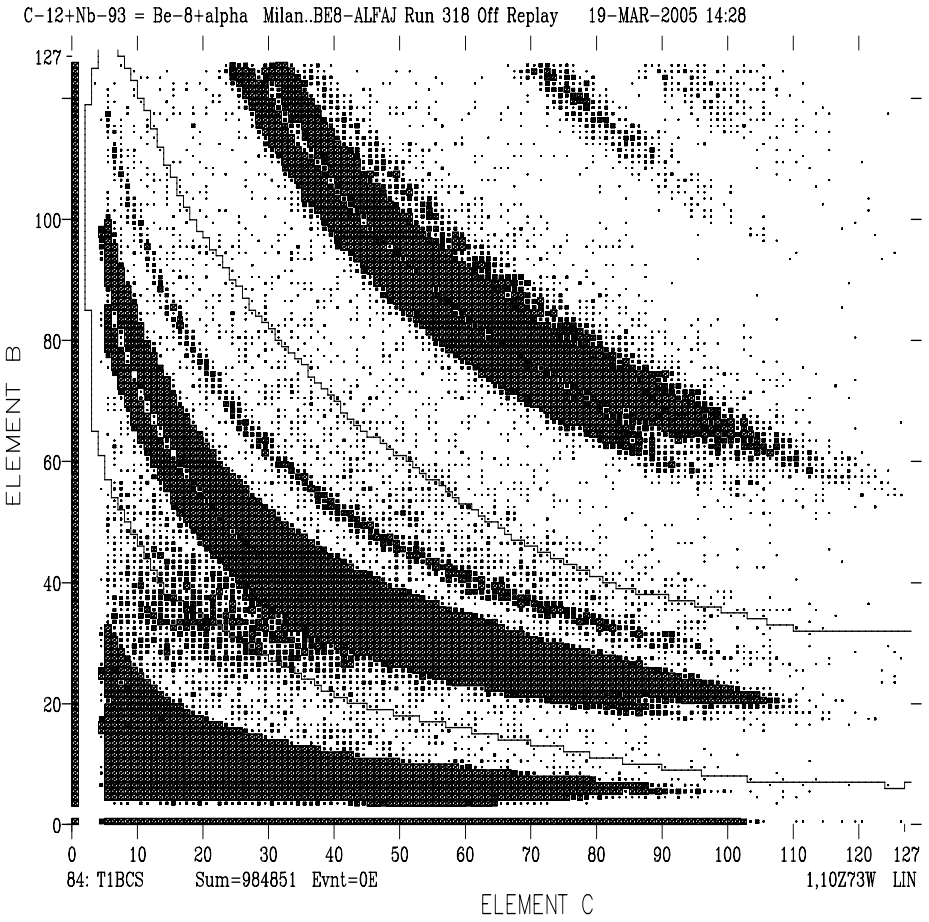

Figure 3.7: Particle identification spectrum of element B versus element C with a gate around the $Z = 2$ loci.

by equation.3.3), which contains ^{3}He, ^{4}He and ^{6}He fragments (see Fig. 3.8), was generated to improve the separation between ^{3}He and ^{4}He. The mass function was generated from the formula given by

$$MF = [(E_B + E_C)^p - (E_C)^p] \times M_s + M_0 \tag{3.1}$$

where,

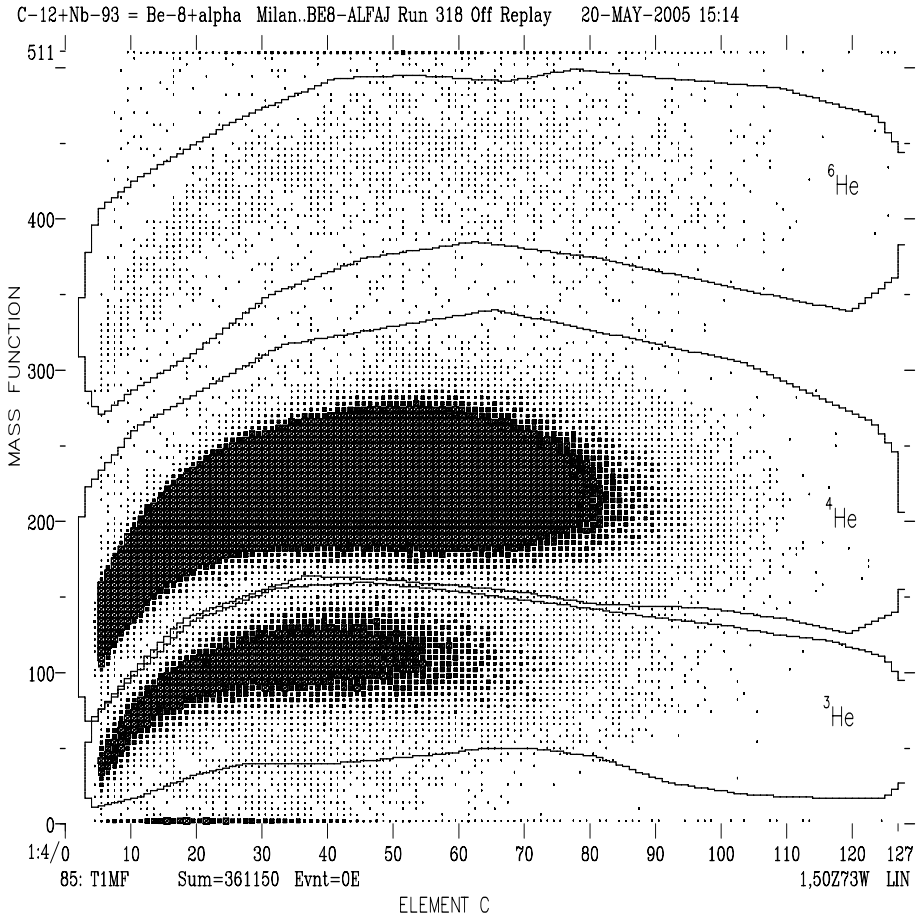

Figure 3.8: Mass function spectrum showing gates that have been set around ^{3}He ,^{4}He and ^{6}He.

$E_B \equiv$ *energy deposited in element* B

$E_C \equiv$ *energy deposited in element* C

$p \equiv$ *constant, its value was found to be 1.7*

$M_s, M_0 \equiv$ *slope and offset parameters obtained from the energy calibrations of elements* B *and* C.

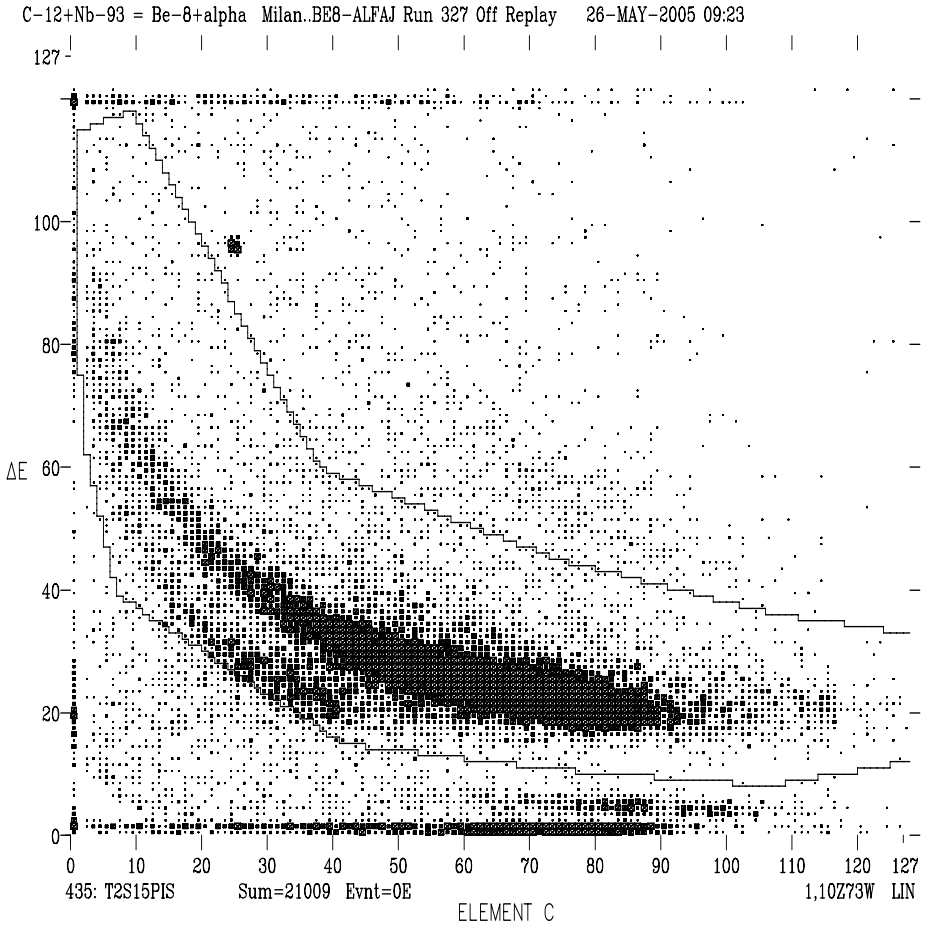

Figure 3.9: Particle identification spectrum showing a gate that has been set around the ^{8}Be events. Events in this gate are mainly the ^{8}Be events. Below this gate are alpha events included in the gate.

3.4.2 Telescope 2

During the analysis Silicon strips 1 and 16 were discarded because they were partially obstructed by the window flanges of the NaI E detector. In the PID of ΔE against element C, a gate has been set around the ^{8}Be events. Events below this gate are the α events (see Fig. 3.9). A mass function was generated for each silicon strip from strips 2 to 15 to separate the ^{8}Be events from the

alpha particles as seen in Fig. 3.10. The energy difference spectrum was

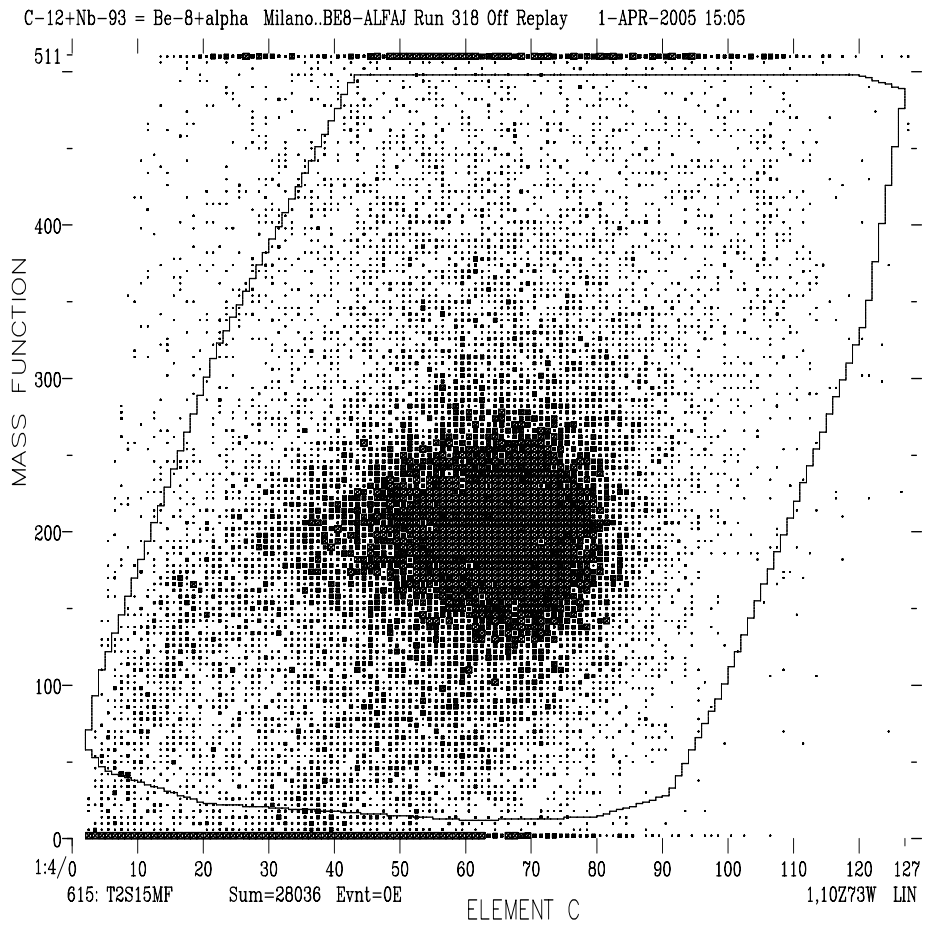

Figure 3.10: Mass function spectrum showing a gate that has been set to separate the ^{8}Be fragments from the alpha particles.

generated to separate contributions from the ground and first excited states of ^{8}Be fragments (see Fig. 3.11). The contribution from the first excited state could not be uniquely separated from events in the ground state. This implies that the energy spectra of the ^{8}Be fragments were extracted with a slight contamination of about 5 % from ^{8}Be fragments in the first excited state.

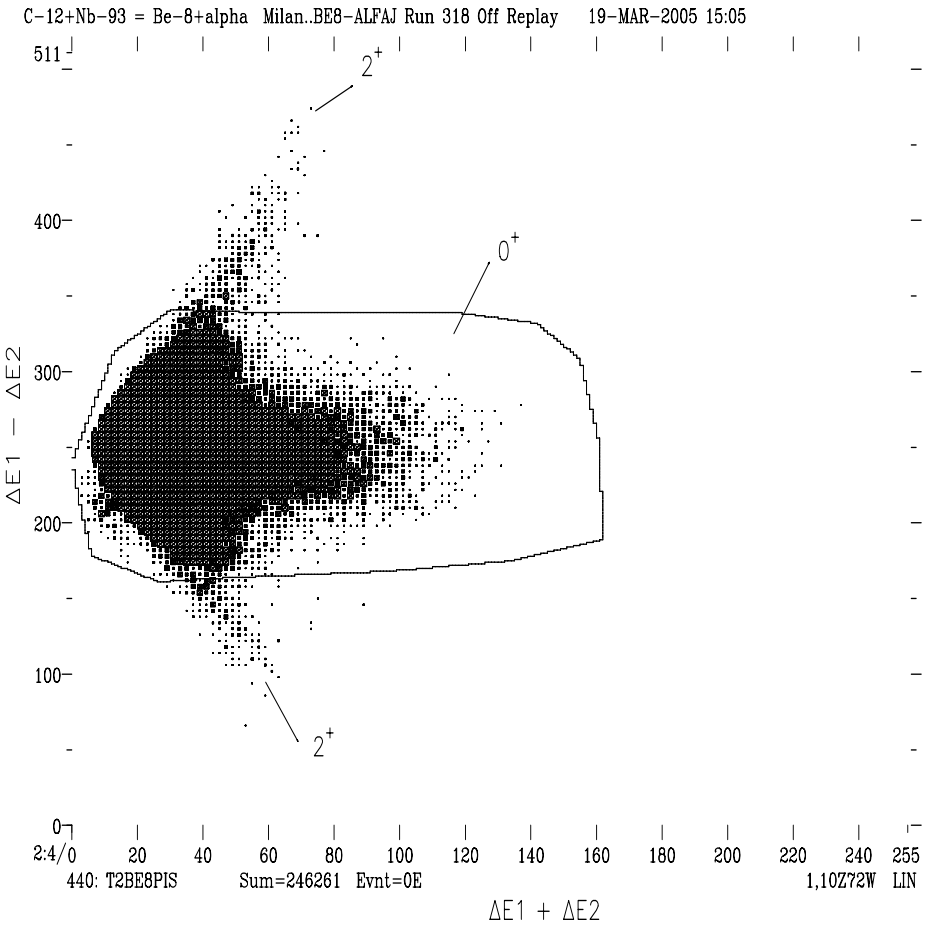

Figure 3.11: Energy difference spectrum showing a gate that is set on the ^{8}Be fragments. The ^{8}Be events in the (0^{+}) and (2^{+}) state are not fully resolved.

3.5 Efficiency calculations for telescope 2

The efficiency of telescope 2 was calculated using a Monte Carlo code (UNIMONTE) [Mac88] developed by the University of Edinburgh. The code was designed to do the Monte Carlo simulations of break-up reactions. The objective of this calculation was to simulate the effective solid angle for the detection of the two correlated alpha particles associated with the ^{8}Be frag-

ment. In order to run the code on the VAX operating system, changes were made within the code, particularly, for the random number generator. Subroutines which were incorporated in the Fortran codes simulate the following:

- angular distribution of break-up fragments
- scattering angular distribution of the ejectile
- excitation distribution of the ejectile
- efficiency of the detector

The details of the reaction and the description of the detector and collimator geometry were defined in the UNIMONTE input file. Two input files, one which handles the kinematics when the ^{8}Be is unbound and the other when the ^{8}Be is assumed to remain as a single cluster, were used.

A total of 100000 events were considered in the calculation. The efficiency of telescope 2 was simulated for 14 strips of the SSD as a function of the excitation energy of the residual nucleus. For the case when the ^{8}Be is bound no corrections for inter-strip gaps were made and no events were discarded. The following types of events were discarded for the case of the unbound ^{8}Be: events when adjacent strips fired, events when there are double hits in a strip and events falling in the inter-strip gaps. The efficiency of the detector was obtained as the ratio of the number of valid events for the case when the ^{8}Be is unbound to the case when ^{8}Be is treated as being bound. The efficiency was used to calculate the effective solid angle of telescope 2 (see equation.3.4) as a function of the ejectile energy.

$$\Omega_{eff} = \Omega \times E_{eff} \tag{3.2}$$

where,

$\Omega_{eff} \equiv$ *is the effective solid angle of telescope 2*

$\Omega \equiv$ *acceptance solid angle of telescope 2*

$E_{eff} \equiv$ *efficiency of telescope 2*

The value of the acceptance solid angle was obtained from

$$\Omega = \frac{A^2}{R} \tag{3.3}$$

where,

$A \equiv$ *surface area of 16 strips*

$R \equiv$ *distance from the target to the strip detector*

Its value was found to be 12.30 $\pm$ 0.02 msr. The detector efficiency as a function of the kinetic energy of ^{8}Be is shown in Fig.3.12.

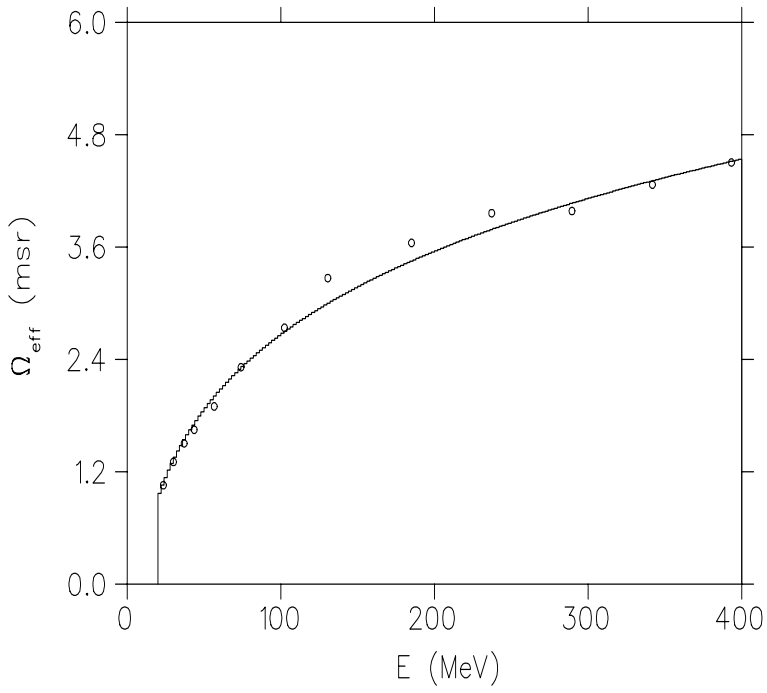

Figure 3.12: Effective solid angle as function of the ^{8}Be kinetic energy in the laboratory system. The points represent results from the current analysis and the histogram represents the average value of the effective solid angle at the center of each bin.

3.6 Error Analysis

3.6.1 Statistical Error

The statistical error arises due to the uncertainty in the number of counts. The statistical error of N number of counts in each bin is defined as $\sqrt{N}$ counts.

3.6.2 Systematic errors

The systematic errors in the double differential cross section spectra are described below and summarized in Table 3.4.

Solid angle

In the case of telescope 1 the uncertainty in the solid angle is due to the uncertainties in the distance from the center of the target to the back of the collimator as well as due to the radius of the collimator. Its value was estimated to be 1.5 %. In the case of telescope 2 the uncertainty in the acceptance solid angle is due to the uncertainty in the distance from the center of the target to the front face of the SSD. Its value was estimated to be 1 %.

Energy calibration

The overall uncertainty in the energy calibration in telescope 1 did not exceed 2 MeV, [Gad99]. That is the uncertainty was estimated to be 1 %. In telescope 2 the uncertainty was estimated to be 5 % because of uncertainties in the thickness of the SSD.

Electronic dead time

The uncertainty in the electronic dead time was calculated and found to be less than 1 %.

Particle identification

The uncertainty in the particle identification was estimated to be 1 % in telescope 1 and to be 5 % in telescope 2. The uncertainty in telescope 2 is large because the ^{8}Be events in the ground state were contaminated by the ^{8}Be events in the first excited state, while in telescope 1, there was a clean separation of the particles.

Current Integrator

The uncertainty in the amount of charge collected by the current integrator was estimated to be less than 2 %.

Target thickness

The uncertainty in the target thickness was estimated to be 5 %.

Total systematic error

3.6.3 Conversion to absolute cross sections

The spectra of the ^{3}He,^{4}He, ^{6}He and ^{8}Be fragments were converted to absolute double differential cross sections by using the equation

$$\frac{d^2\sigma}{d\Omega dE} = N_C \cdot F \cdot K \tag{3.4}$$

where,

$N_C \equiv$ is the number of counts in each bin and F is the normalization factor calculated from

Table 3.3: Total systematic errors

	Telescope 1	*Telescope 2*
Source	*Error %*	*Error %*
Solid angle	1.5	1
Target thickness	5	5
Electronic dead time	1	1
Energy calibration	1	5
Particle identification (PID)	1	5
Current integrator	2	2
Total systematic error	5.852	9.00

$$F = \frac{1}{d\Omega \cdot dE \cdot D_T \cdot N_O \cdot \rho} \tag{3.5}$$

where,

$\Omega \equiv$ *solid angle in sr*

$E \equiv$ *bin size in MeV*

$D_T \equiv$ *electronic dead time*

$N_O \equiv$ *number of* ^{12}C *nuclei in the beam*

$\rho \equiv$ *number of nuclei per unit area of target thickness in mb*

The inclusive spectra of the ^{3}He and ^{6}He fragments were used to calculate absolute cross sections by using the normalization factor applied to the double differential cross section spectra of the alpha particles measured in the alpha telescope. The value of the normalization parameter K, obtained by overlaying the current data onto the existing singles data set, was found to be 15.725 on average which is consistent with the prescaling factor for the prescaled singles events.

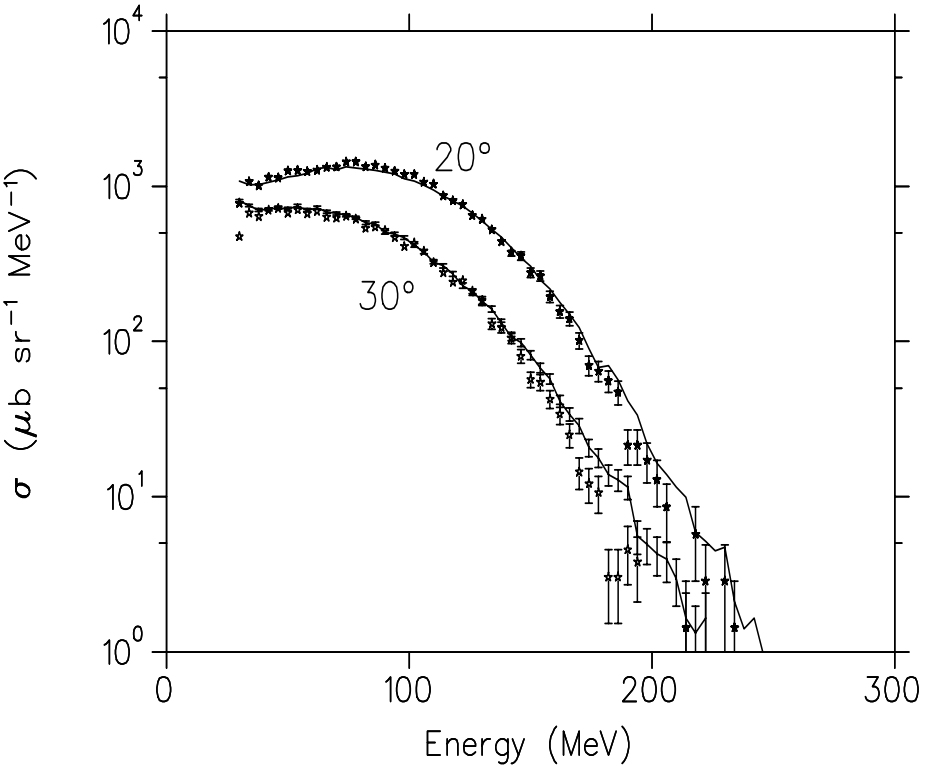

Figure 3.13: Comparison of the double differential cross section spectra of ^{3}He particles emitted in the interaction of ^{12}C with ^{93}Nb at 400 MeV incident energy with available ^{3}He data from the interaction of ^{14}N with ^{93}Nb at 400 MeV energy. The diamonds represent the current results while the curves represent the ^{3}He data obtained from the ^{14}N study.

3.6.4 Normalization of ^{3}He data

In order to check the normalization of ^{3}He data obtained in this study, they were overlaid on the existing singles data set obtained from the interaction of ^{14}N with ^{93}Nb at 400 MeV at the emission angles of 20° and 30° (see Fig. 3.13.). Clearly, Fig.3.13 shows that there is a good qualitative as well as quantitative agreement between these data. Thus, it can be concluded that the energy calibrations and absolute normalization of ^{3}He is consistent with

the absolute normalization of ^{4}He particles.

Chapter 4

Theory

4.1 Introduction

The energy spectra of the IMF's and particles emitted in the interaction of ^{12}C with medium mass target nuclei were previously reproduced by means of a theoretical model that is been developed at the University of Milan ([Bec03] [Gad99] [Gad01]). In the present study this model has been extended to include also the emission of ^{3}He and ^{6}He particles. In the model it is considered that, prior to break-up, the projectile may suffer a considerable energy loss in an initial state interaction by means of a nuclear friction dissipative mechanism which excites the target nucleus. The aim of the theoretical analysis was to check what role break-up and nucleon coalescence contributions play in the emission of ^{3}He and ^{6}He in the interaction of ^{12}C with ^{93}Nb at an incident energy of 400 MeV.

In this study the first mechanisms, i.e. projectile break-up, is described within the Serber approximation [Ser47]. The second mechanisms, nucleon coalescence, is described within the framework of the Boltzmann Master equation [Cav01], [Cav98], [Cav97], [Cav96]. In this chapter a detailed de-

scription of the projectile break-up and nucleon coalescence mechanisms are given.

4.2 The projectile break-up Mechanism

The spectra of break-up fragments were evaluated by folding the LPWA [McV80] with an exponential survival probability([Gad01], [Gad99]. The survival probability $P(E_1) = 1$ was assigned for values of E_L below the energy loss threshold $E_{L,min}$, hence the break-up cross section should be zero. As described in the Serber-McVoy-Hussein hypothesis ([Gad01] [Gad99]) the multiplicity spectra, $\frac{d^2\sigma}{d\Omega dE'}(E, E', \Theta)$, of the emitted fragments with energy E' produced when the ^{12}C initial kinetic energy in the center-of-mass, E_0, was reduced to $E = E_0$ - E_1, is evaluated by correcting the energy of the observed fragment for the Coulomb repulsion, at the moment of break-up. Therefore, the break-up fragment's cross section is obtained from the formalism

$$\frac{d^2\sigma}{dEd\Omega}(E_0, E', \theta) = \sigma_{bu}\frac{\int_0^{E_0} P(E_1)S(E, E', \theta)dE_1}{\int_0^{E_0} P(E_1)dE_1} \tag{4.1}$$

where,

$\sigma_{bu} \equiv$ *is the energy integrated break-up cross section for the production of break-up fragments*

Assuming a constant projectile energy loss per unit length $\frac{dE}{dx} = 1/k$ and a constant break-up and mass transfer probability kk' per unit length, the ^{12}C survival probability after an energy loss E_l is given by

$$P(E_1) \propto exp[-kk'(E_1 - E_{1,min})] \tag{4.2}$$

Also,

$$P(E_1) = 1, for\ E_1 < E_{1,min} \tag{4.3}$$
$$P(E_1) = exp[-kk'(E_1 - E_{1,min})], for\ E_{1,min} \leq E_1 \leq E_0 \tag{4.4}$$

The cross section for producing a fragment of energy E' at an angle θ in the break-up of the projectile of energy $E = E_o - E_1$ is given by

$$S(E, E', \theta) = 0, for\ E_1 < E_{1,min} \tag{4.5}$$

$$S(E, E', \theta) = \frac{d^2\sigma^s(E, E'\theta)}{dE'd\Omega}, for\ E_1 \geq E_{1,min} \tag{4.6}$$

In the local plane wave approximation (LPWA) [Ser47] [McV80] the double differential cross sections were evaluated by

$$\frac{d^2\sigma^s}{d\Omega dE} \propto P'P''|\psi(p)|^2 \tag{4.7}$$

where,

$$\psi(\mathbf{p}) = \frac{1}{(2\pi\hbar)^{3/2}} \int \psi(r) exp[\frac{-i}{\hbar}\mathbf{p} \cdot \mathbf{r}]d\mathbf{r} \tag{4.8}$$

is the Fourier transform (L = 0, L is the angular momentum of the fragment) [Gad99] of the wave function $\psi(r)$ which describes the fragment's relative motion inside the projectile and the internal momentum distribution of the fragment inside the projectile is given by

$$\mathbf{p} = \mathbf{P'} - (\frac{m_f}{m_p})\mathbf{P} \tag{4.9}$$

where,

$p \equiv$ *is the momentum of the projectile when it breaks-up, i.e after energy loss*

$P' \equiv$ *momentum of the observed fragment just after break-up*

$P'' \equiv$ *momentum of the unobserved fragment*

For $(L \geq 1)$, the square of the Fourier transform is well reproduced by the expression [Bal64] given by

$$|\psi(p)|^2 = p^{2L} exp(-p^2/2P_L^2) \tag{4.10}$$

The double differential spectra of the break-up fragments is predicted by the deuteron-like wave function of the form

$$\psi(r) = \frac{R(r)}{r}, \tag{4.11}$$

where,

$$\begin{aligned} R(r) = Ar^2, 0 \leq r \leq b+f, \\ BsinK(r-b), b+f < r \leq b+R, \\ Ce^{-r/R_0}, r > b+f \end{aligned} \tag{4.12}$$

where,
$K = \frac{\sqrt{2\mu(V_0-B)}}{\hbar}$

The quantities f and R_o are free parameters, while $b = (2tanKf - Kf)/k$, and $R = 1/Karctan(-KR_0)$

The values of the constants A, B and C given by their matching and normalization conditions are

$$A = B\frac{sinKf}{(b+f)^2}, \tag{4.13}$$

$$B = \frac{1}{2\sqrt{\pi}}\sqrt{\frac{1}{\frac{b+f}{5}sin^2Kf + 1/2(R-f) - 1/4K(sin2KR - sin2Kf) + \frac{R_o}{2}sin^2KR}}, \tag{4.14}$$

$$C = Be^{b+R/R_o} sinKR \tag{4.15}$$

The corresponding fourier transform for the fragments's relative motion inside the projectile is

$$\begin{aligned}\psi(\mathbf{p}) = \frac{4\pi B(\hbar c)^2}{(2\pi\hbar)^{3/2}} \frac{1}{pc} \frac{sinkf}{pc} [\frac{2(\hbar c)^2}{(pc)^2(b+f)^2}(cos\frac{pc(b+f)}{\hbar c} - 1) \\ -cos\frac{pc(b+f)}{\hbar c} + \frac{2\hbar c}{pc(b+f)} sin\frac{pc(b+R)}{\hbar c}] \\ + \frac{1}{(\hbar Kc)^2 - (pc)^2} [pcsinKRcos\frac{pc(b+R)}{\hbar c} - \hbar Kccos KRsin\frac{pc(b+R)}{\hbar c} \\ -pcsinKfcos\frac{pc(b+f)}{\hbar c} + \hbar cKcosKfsin\frac{pc(b+f)}{\hbar c}] \\ + \frac{sinKR}{(\hbar c/R_0)^2 + (pc)^2} [pccos\frac{pc(R+b)}{\hbar c} + \frac{\hbar c}{R_0} sin\frac{pc(R+b)}{\hbar c}]\end{aligned} \tag{4.16}$$

The angular and energy distribution of the emitted fragments, and the angular distribution of the intermediate excited system created when the complementary fragment fuses with target, may be evaluated by assuming that the incident projectile is slowed down by the Coulomb barrier between the projectile and the target nucleus, and that the energy of the projectile is shared amongst the two fragments [Ser47]. This is given by the expression

$$\frac{d^2\sigma}{dE_s d\Omega_s} \propto \frac{\sqrt{E_s E_P}}{2\mu B_P + (\frac{2{m_a}^2 E_p}{m_P} + 2m_a E_a - 4\sqrt{\frac{{m_a}^3}{m_P}}\sqrt{E_P E_a} cos\theta)^2} \tag{4.17}$$

where, a is the spectator fragment (which flies away), b is the participant fragment (which fuses with the target), E_a and E_b are their kinetic energies, B_P is the binding energy of a and b inside the projectile P, μ is the reduced mass of the system $(a+b)$, m_P, m_a, and m_b are the masses of P, a, and b, respectively, and θ is the emission angle of a with respect to the direction of the projectile P.

4.3 Re-emission of alpha particles after incomplete fusion

During the incomplete fusion of the projectile fragments with the target nucleus one of the fragments (spectator fragment) comes out while the other (participant fragment) is absorbed by the target nucleus. The absorbed fragment may be re-emitted only after a few interactions with the target nucleons, but with a large fraction of its initial energy [Gad99]. The re-emission of the absorbed fragment occurs at peripheral regions of the target nucleus. The absorbed fragment may be re-emitted with an enhanced probability because it may be scattered towards even more peripheral nuclear regions. The angular distribution of the re-emitted alpha particle after its incomplete fusion can be reproduced from the equation

$$\frac{d^2\sigma}{dEd\Omega} = Ce^{-(\theta/\Delta\theta)} \tag{4.18}$$

where,

$\Delta\theta \equiv = 2\pi/K\Delta R$

$K \equiv$ *alpha-particle wave number*

$\Delta R \equiv$ *thickness of a nuclear surface where* α*-nuclear collision occur*

$C \equiv$ *is a constant*

where,

$$\Delta R = cA^{1/3} \tag{4.19}$$

where,

$c \equiv$ *denotes the fitting parameter of the angular distributions which depends on the energy of the alpha particle before and after scattering and also*

on the nucleon Fermi energies
$A \equiv$ mass of an alpha particle

4.4 Nucleon Coalescence

4.4.1 BME theory of pre-equilibrium emission

The evolution of the composite system towards statistical equilibrium, after the complete fusion of the projectile with the target nucleus and the incomplete fusion of the projectile fragment with the target nucleus, is evaluated by solving a set of coupled master equations, (BME) [Cav96], [Cav97], [Cav98], [Cav01]. The evolution is simulated by defining a set of bins which have a constant volume in momentum space. If mean values are considered one may assume azimuthal symmetry with respect to the beam direction, and can then use only two independent variables, p^2 and p_z, which describe the square of the nucleon's momentum and the component of the linear momentum along the beam axis. With this assumption the momentum bins are characterized by constant values of Δp^2 and Δp_z.

The nucleon states, described as two fermion gas, are classified according to their energy ϵ and divided into bins of width $\Delta\epsilon$. The occupation numbers for the proton and neutron gas within bin i are defined by the expression

$$\begin{aligned}\frac{d(n_i g_i)^\pi}{dt} = &\sum_{jlm} \omega^\pi_{lm\to ij} g^\pi_l n^\pi_l g^\pi_m \; n^\pi_m (1-n^\pi_i)(1-n^\pi_j) \\ &-\omega^{\pi\pi}_{ij\to lm} g^\pi_i n^\pi_i g^\pi_j n^\pi_j (1-n^\pi_l)(1-n^\pi_m) \\ &+\sum_{jlm} \omega^{\pi\nu}_{lm\to ij} g^\pi_l n^\pi_l g^\nu_m n^\nu_m (1-n^\pi_i)(1-n^\nu_j) \\ &-\omega^{\pi}{}_{ij\to lm} g^\pi_i n^\pi_i g^\nu_j n^\nu_j (1-n^\pi_l)(1-n^\nu_m) \\ -n^\pi_i g^\pi_i \omega^\pi_i \to_{i'} \; &g^\pi_{i'} \delta(\epsilon^\pi_i - \epsilon^\pi_F - B^\pi_i - \epsilon^\pi_{i'}) - \frac{dD^\pi_i}{dt}\end{aligned}$$

The parameters π and ν represent the protons and neutrons, respectively. The unstable nucleons may escape from the nucleus with energy

$$\epsilon_{i'} = \epsilon_i - \epsilon_f - B_i \tag{4.20}$$

where, ϵ_f and B_i are the fermi and binding energies of the nucleons in the compound nucleus. The nucleons which escape from the nucleus with energy $\epsilon_{i'}$ lead to pre-equilibrium particle emission. The quantities $\omega_{ij} \rightarrow_{lm}$, $\omega_i \rightarrow_{i'}$ and $\frac{dD_i^{\pi}}{dt}$ represent the internal transition decay rates, the decay rates for emission of single protons into the continuum, and a depletion term which considers the emission of protons bound in clusters.
The internal transition rates are given by

$$\omega_{ij} \rightarrow_{lm} = \frac{1}{2\pi} \int_0^{2\pi} \omega_{ij} \rightarrow_{lm} d\Phi_j, \tag{4.21}$$

where,

$$\omega_{ij} \rightarrow_{lm} = \frac{\sigma_{ij}\nu_{ij}\Pi_{ij} \rightarrow_{lm}}{V} \tag{4.22}$$

where,
$V \equiv$ *is the nuclear volume*
$\nu_{ij} \equiv$ *is the two nucleon relative velocity*
$\sigma_{ij} \equiv$ *interacting cross section between nucleons with momenta* P_i *and* P_j

The indeces i, j, l, m represent the momenta for p_i, p_j, p_l, p_m and Φ_j is the azimuthal angle of p_j. The quantity $\Pi_{ij} \rightarrow_{lm}$ represents the probability of reaching bins l and m if the interacting nucleons have momenta p_i and p_j belonging to bins i and j.
The decay rates $\omega_i \rightarrow_{i'}$ are given by

$$\omega_i \rightarrow_{i'} = \frac{\sigma_{inv}\nu_i'}{g_i V'} \tag{4.23}$$

where,

$\sigma_{inv} \equiv$ *is the inverse cross section*

$\nu'_i \equiv$ *is the relative velocity between the nucleon and the residual nucleus, when neglecting that the nucleus recoils, this coincides with the nucleon velocity with respect to the center of mass system*

$V' \equiv$ *is the laboratory volume which cancels the same factor appearing in the expression of* g'_i

$g_i \equiv$ *total number of states in bin* i

The multiplicity spectra of the particles emitted in the time interval dt at an angle θ with energy E' is given by

$$\frac{d^3N'(E',\theta,t)}{dE'd\theta dt} = RN(\epsilon,\theta,t)\frac{\sigma_{inv}\nu'_i}{V'}\rho(E',\theta) \tag{4.24}$$

where,

$E' \equiv$ *is the energy of the emitted particle into the continuum*

$N(\epsilon,\theta,t) \equiv$ *is the occupation probability of the states of the considered particle inside the composite nucleus*

$R \equiv$ *is the survival factor that takes into account the possible dissolution of the cluster before emission*

$\rho(E',\theta) = \frac{sin\theta}{2}\rho E'$

where $\rho(E')$ is the density of the particle states in the continuum.

The measured multiplicity spectra are given by

$$\frac{d^2M_C}{dE'd\Omega}(E'_C,\theta_C) = \frac{R_C}{2\Pi\sin\theta}\int N_C(E'_C,\theta_C,t)\frac{\sigma_{inv,C}\nu_C}{V}\rho_C(E'_C,\theta_C)dt \tag{4.25}$$

where, R_C is the probability for emission of the cluster before it dissolves into its constituent nucleons. Assuming Q_c is the q-value for the cluster emission and $A_c = N_c + Z_c$, then the continuum energy of the cluster C is given by

$$E_c' = E_c + Q_c - A_c(\epsilon_f - \epsilon_{cf}) \tag{4.26}$$

where ϵ_f and ϵ_{cf} are the composite nucleus and the cluster fermi energies.

The direction for the clusters with energy E_c inside the nucleus which forms an angle θ_c with respect to the beam is given by

$$N_C(E_C, \theta_C, t) = \pi_i(n_i^\pi)^{p_i}(E_C, \theta_C) Z_C \cdot \Pi_i(n_i^\nu)^{p_i}(E_C, \theta_c) N_C \tag{4.27}$$

where the index i runs over all bins in which the nucleons constituting the cluster may be found and $P_i(E_C, \theta_C)$ is the fraction of bin i within the Fermi sphere of the cluster C with radius p_{cf}.

4.4.2 Modified BME

The set of equations mentioned in the preceding sections can be modified such that indeces i, j, l, m refer to angles as well as to energies. To solve these equations, the momentum space is divided into bins with

$$p_i^2 - \frac{\Delta p_i^2}{2} \leq p^2 < p_i^2 + \frac{\Delta p_i^2}{2} p_{i,z} - \frac{\Delta p_{i,z}}{2} \leq p_z < p_{i,z} + \frac{\Delta p_{i,z}}{2} \tag{4.28}$$

where,

$p^2 \equiv$ *modulus square of the nucleon momentum*

$p_z \equiv$ *its component along the beam direction*

The relative velocity of the two nucleons representing the probability of reaching particular pairs of bins is calculated as a ratio of the area Δ_{al}, on a sphere S. The area Δ_{al} is evaluated from

$$\Delta_{al} = \Delta_a \cdot \Delta_l, \tag{4.29}$$

with

$$\Delta a = [p_l^2(\Delta\theta_l)^2 + p_l^2 sin^2\theta_l(\Delta\phi_l)^2]^{\frac{1}{2}}, \tag{4.30}$$

$$\Delta_l = \frac{\Delta_{pl}}{sin\alpha} \tag{4.31}$$

The angle ϕ_l is the azimuthal angle of p_l, the possible final momentum in bin l following the interaction of the two nucleons with momenta p_i and p_j and is given by the expression

$$\phi_l = arccos\frac{(P^2 + p_l^2 - p^2) - 2Pp_l cos\theta cos\theta_l}{2Pp_l sin\theta sin\theta_l} \tag{4.32}$$

where,

$\theta = arccos\frac{P_z}{P}$

$P_z \equiv$ *is the z-component of* P

The center of mass multiplicity spectra of the emitted nucleons and clusters are given by

$$\frac{dN_{i,c}^3}{d\theta_i dE_i dt}(\theta_i, E_i) = N_i(\theta_i, E_i)\frac{\sigma_{inv}\nu'}{\Omega}\rho(E_{i'}) \tag{4.33}$$

where,

$N_i(\theta_i, E_i) \equiv$ *is the nucleon or cluster occupation number*

$\sigma_{inv} \equiv$ *emitted nucleon or cluster inverse cross section*

$\nu' \equiv$ *ejectile-residual nucleus relative velocity*

$\rho(E_{i'}) \equiv$ *is the ejectile continuum state density*

4.4.3 Energy distribution in BME theory

The evaluation of the internal momentum distribution of the fragments within the projectile depends on the distribution function. The choice of the distribution function depends on the mass, A, of the projectile or the target

nucleus, or in the case of the projectile on the incident energy of the projectile. For A $\leq$ 40 a Gaussian distribution function (G) is used while for A $<$ 40 a Saxon Wood distribution (SW) is used. The nucleon momentum density distributions are calculated with a SW function which takes a form

$$\rho(p) \sim [1 + exp(\frac{(p - p_0)}{\Delta p})]^{-1} \tag{4.34}$$

The nucleon momentum density distributions are calculated with a G of the form

$$\rho(p) \sim [-exp(\frac{(p - p_0)}{\Delta p})^2] \tag{4.35}$$

where p_0 and Δp are the initial internal momentum distribution inside the projectile and the target nucleus, respectively.

The emitted fermi cluster energies were evaluated by using values obtained from the liquid drop model. That is,

$$\bar{\epsilon_f} = \frac{1}{A}[ZE_{f_Z} + NE_{f_N}], \tag{4.36}$$

where,

$E_{f_Z} \equiv$ *fermi energy of the cluster's protons*

$E_{f_N} \equiv$ *fermi energy of the cluster's neutrons*

The fermi energy of the cluster's protons and neutrons are evaluated from

$$E_{f_Z} = E_f(\frac{2Z}{A})^{2/3}(1 - 0.3867A^{-1/3})^2 \tag{4.37}$$

$$E_{f_N} = E_f(\frac{2N}{A})^{2/3}(1 - 0.3867A^{-1/3})^2 \tag{4.38}$$

The effective coulomb barrier V_c which the cluster feels at the moment of emission was evaluated using the semi-classical inverse cross sections. Thus, for the emitted cluster, the inverse cross section is given by

$$\sigma_{inv,c} = \sigma_{geo}(\theta)(1 - \frac{V_c(\theta)}{E_{ch}}), \tag{4.39}$$

where, $\sigma_{inv,c}$ is the cluster's inverse cross section, $V_c(\theta)$ and $\sigma_{geo}(\theta)$ are the Coulomb barrier and the geometrical cross section in the recoiling nucleus reference frame , which due to nuclear deformations depends on the emitted particle's emission angle. In order to take into account the possibility of cluster emission below and around the Coulomb barrier, the inverse cross sections were evaluated using an expression contained within the Hill and Wheeler parabolic approximations [Hil53].

4.4.4 Mean field interaction

Nuclear mean field effects are still dominant at the early stages of the reaction even at incident energies of a few MeV/n. At above 10 MeV/n subsequent stages of the reaction the dynamics are strongly governed by two-body interactions and the mean field plays a less important role [Bru95]. A Vlasov-Uehling-Uhlenbeck (VUU) theory applied by Bertsch et al., [Ber88] which takes into account the competition between one-body and two-body interactions has been considered to provide a clear description of the reaction dynamics in the intermediate energy regime. The mean field effects at the initial stage of the reaction around the collision time t_{coll} were obtained by solving the Vlasov predictions with the laboratory values given by [Bru95]

$$P_P^t = [\frac{2m(E_{Lab} + \frac{A_C}{A_T}Q)}{A_P}]^{1/2}\frac{A_T}{A_C} \tag{4.40}$$

which describes the projectile nucleons, while the target nucleons are described by the equation

$$P_T^t = [\frac{2m(E_{Lab} + \frac{A_C}{A_T}Q)}{A_P}]^{1/2}\frac{A_P}{A_C} \tag{4.41}$$

where,

$A_C \equiv$ *is the mass number of the composite nucleus*

$E_{Lab} \equiv$ *is the beam energy in the laboratory system*

$m \equiv$ *is the nucleon mass number*

$Q \equiv$ *is the fusion Q-value*

The increase in the total kinetic energy can be viewed as collective kinetic energy to be supplied to the centers of the mass of the projectile and the target. Thus the projectile and target translational momenta, in terms of an effective incident energy, are obtained by substituting E_{Lab} in equations 4.40 and 4.41 by

$$E_{Lab}^{eff} = E_{Lab} + S \tag{4.42}$$

where S include the acceleration due to the change of the potential well and is calculated from

$$S = \frac{A_C}{A_T}[\frac{3}{5}A_P(\bar{\epsilon}_{f_C} - \bar{\epsilon}_{f_P}) + \frac{3}{5}A_T(\bar{\epsilon}_{f_C} - \bar{\epsilon}_{f_T})] \tag{4.43}$$

where P, T and C represent the projectile, target and composite nucleus and $\bar{\epsilon}_f$ are the Fermi energies of the projectile, target nucleus, and composite nucleus, respectively.

Chapter 5

Results and Discussion

5.1 Overview

This chapter presents the experimental and theoretical results of the inclusive spectra of ^{3}He and ^{6}He. The measured spectra of these fragments are compared with the ^{4}He spectra to confirm the presence of the projectile fragmentation and nucleon coalescence mechanisms. Further, the previous calculations are extended to also describe ^{3}He and ^{6}He.

5.2 Inclusive spectra of ^{3}He and ^{6}He

5.2.1 Measured spectra of ^{3}He and ^{6}He

The measured inclusive absolute normalized cross section spectra of the fragments of ^{3}He and ^{6}He are shown in Fig.5.1 and Fig.5.2, respectively.

The distinction between these spectra is that the ^{3}He spectra show an almost isotropic distribution at the emission angles studied, while the ^{6}He spectra vary with emission angle. The measured absolute spectra of the alpha particles have been compared with the spectra of ^{3}He and ^{6}He particles, of

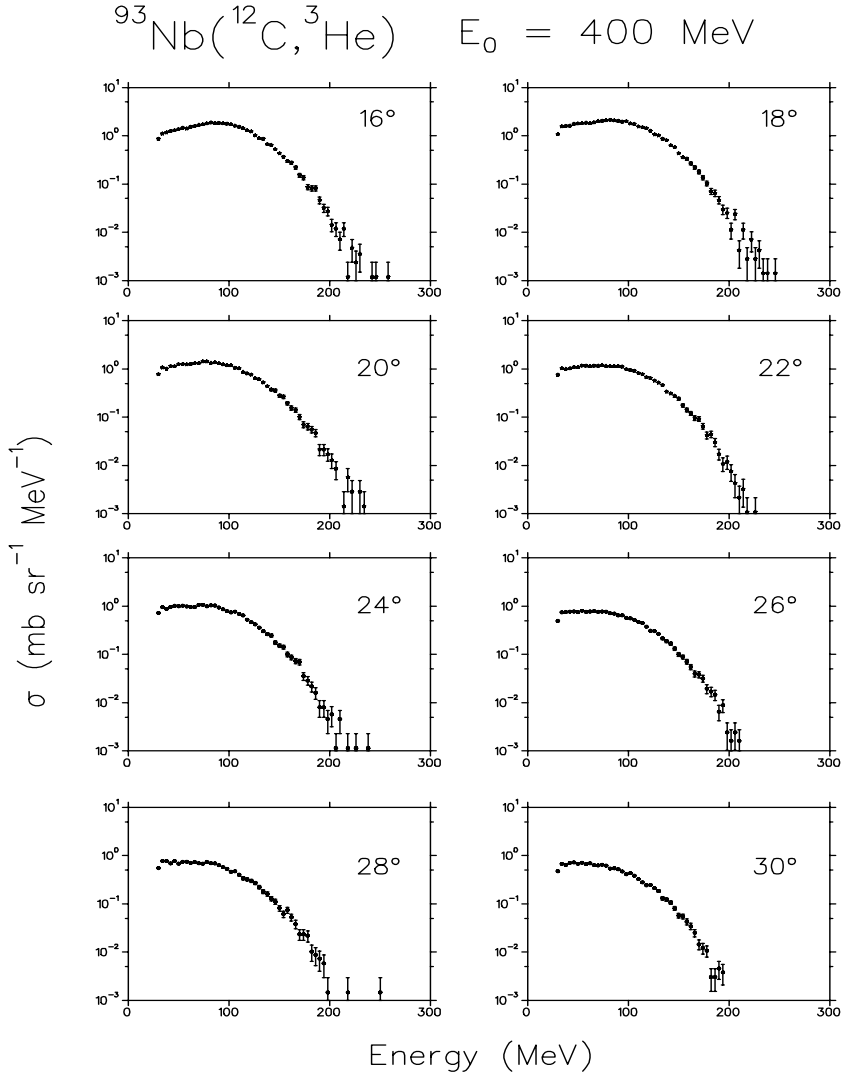

Figure 5.1: Measured absolute cross-sections of ^{3}He fragments at eight emission angles in the lab system. The error bars reflect the statistical error.

which the results are shown in Fig.5.3.

The ^{3}He and ^{6}He fragments are produced with smaller cross sections. The ^{3}He and ^{6}He spectra (Fig.5.3) exhibit features which are interpreted as contributions from both mechanisms. These mechanisms were used previously

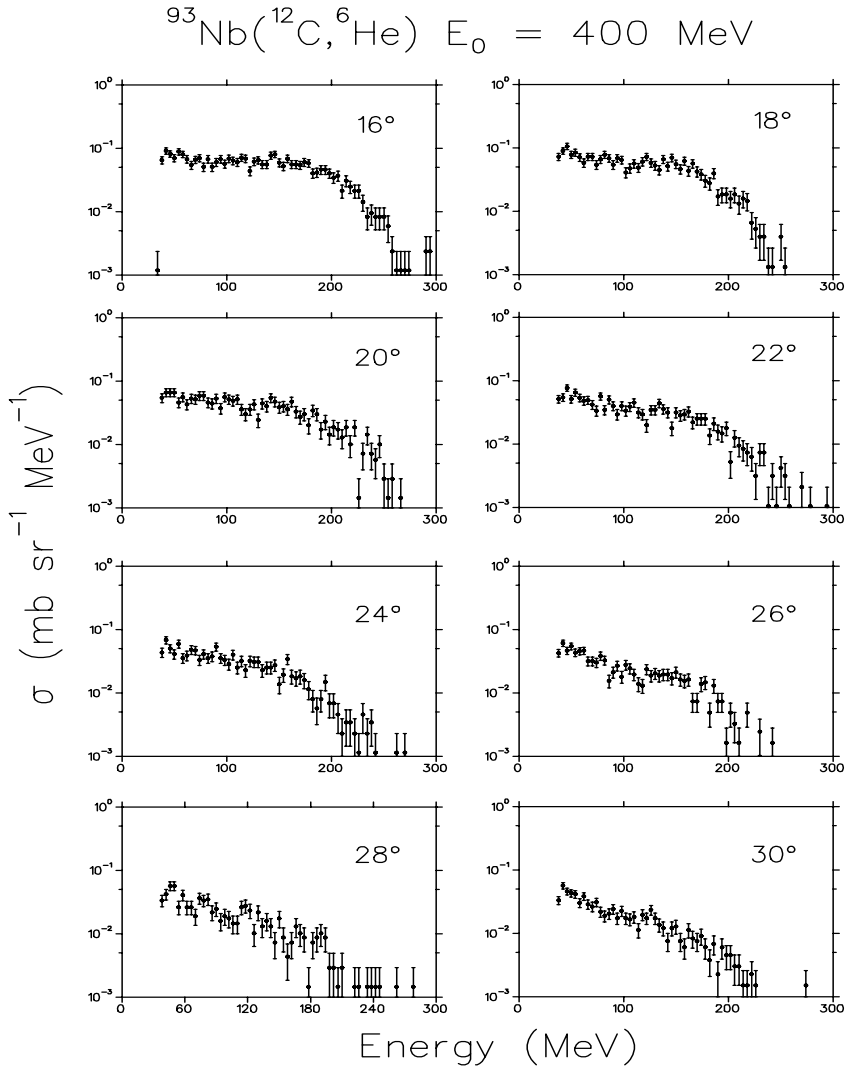

Figure 5.2: Measured absolute cross-sections of the ^{6}He fragments at eight emission angles in the lab system. The error bars reflect the statistical error.

to explain some of the features in the spectra of ^{4}He particles and other intermediate mass fragments.

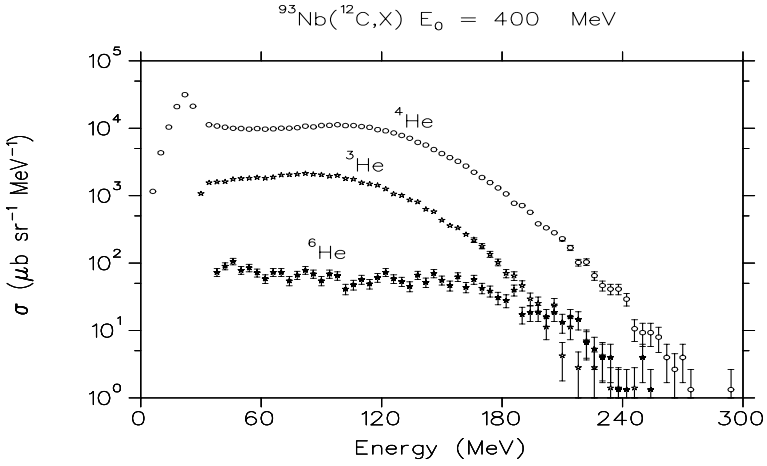

Figure 5.3: Measured absolute cross-sections of the ^{3}He, ^{4}He and ^{6}He fragments at an emission angle of 18°. The error bars reflect the statistical error.

5.2.2 Theoretical calculations

In order to reproduce the experimental normalized absolute cross-sections, the contributions from the coalescence and break-up mechanisms were normalized by the complete and incomplete fusion cross-sections, respectively. These were found to be 95 mb and 5 mb for ^{3}He and ^{6}He, respectively. The value of the incomplete fusion cross section in the case of ^{3}He is the same as the value found in the analysis of the complementary ^{9}Be fragment. For the ^{6}He fragment, the value of the incomplete fusion cross section is small and is consistent with the trend suggested by the break-up of ^{12}C into $He - Be$ fragments. The coalescence contribution for both nuclei was evaluated by considering the complete fusion of the projectile with the target nucleus while the break-up contribution was evaluated based on the incomplete fusion of the unobserved participant fragment with the target nucleus.

The results presented in Fig.5.4 and Fig.5.5 are for the break-up and coalescence contributions, respectively. The coalescence cross section are cal-

culated in the centre of mass system while the final results are presented in the laboratory system.

5.3 Discussion

In order to interpret the measured results in relation to the theoretical calculations, the ^{3}He and ^{6}He nuclei were treated differently in the code. For a ^{3}He nucleus, a Balashov potential with $L = 1$ was used to describe the fragment's relative motion within the projectile, while for a ^{6}He fragment, a square well approximation with a depth of 65 MeV was used. The theoretical analysis of these fragments also considered the dominance of the initial state interaction of the projectile with an energy loss, E_l, of 98 MeV for ^{3}He, 92 MeV for ^{6}He, and 120 MeV for ^{12}C. The value of the energy loss E_l in the case of ^{3}He is large compared to the energy loss of ^{9}Be fragment (49 MeV) and is consistent with a distant collision when the fusing fragment has a smaller mass. In the case of ^{6}He, the value of E_l is the same as the value found in the previous analysis of the fragmentation of ^{12}C into ^{7}Be and ^{5}He.

The spectra of ^{3}He and ^{6}He fragments are presented in Figs.5.6 and 5.7. In these figures the theoretical results presented as incoherent sum of both contributions, have been compared to the measured spectra, see Fig. 5.6 and Fig. 5.7. A similar trend is exhibited by the results of both fragments. The calculations could reproduce the distribution widths of these spectra when a break-up mechanism was assumed. However, the calculations did not reproduce the lower-energy component of the spectra, assuming the break-up mechanism. This feature of the spectrum could be explained in terms of nucleon coalescence during the thermalization of the intermediate excited nuclei created in the complete fusion of the projectile with the target or the incomplete fusion of the projectile fragment with the target nucleus.

Both the measured and theoretical results of ^{3}He show that the relative strengths of the break-up and coalescence contributions do not depend on the emission angle. However, for the ^{6}He nuclei the break-up contribution decreases gradually with emission angle whereas the coalescence mechanism does not vary with emission angle. These differences could be explained as due to their production cross sections which are small compared to the production cross sections for the alpha particles. This suggests that the binary break-up of ^{12}C is more likely to produce an α and a ^{8}Be fragment.

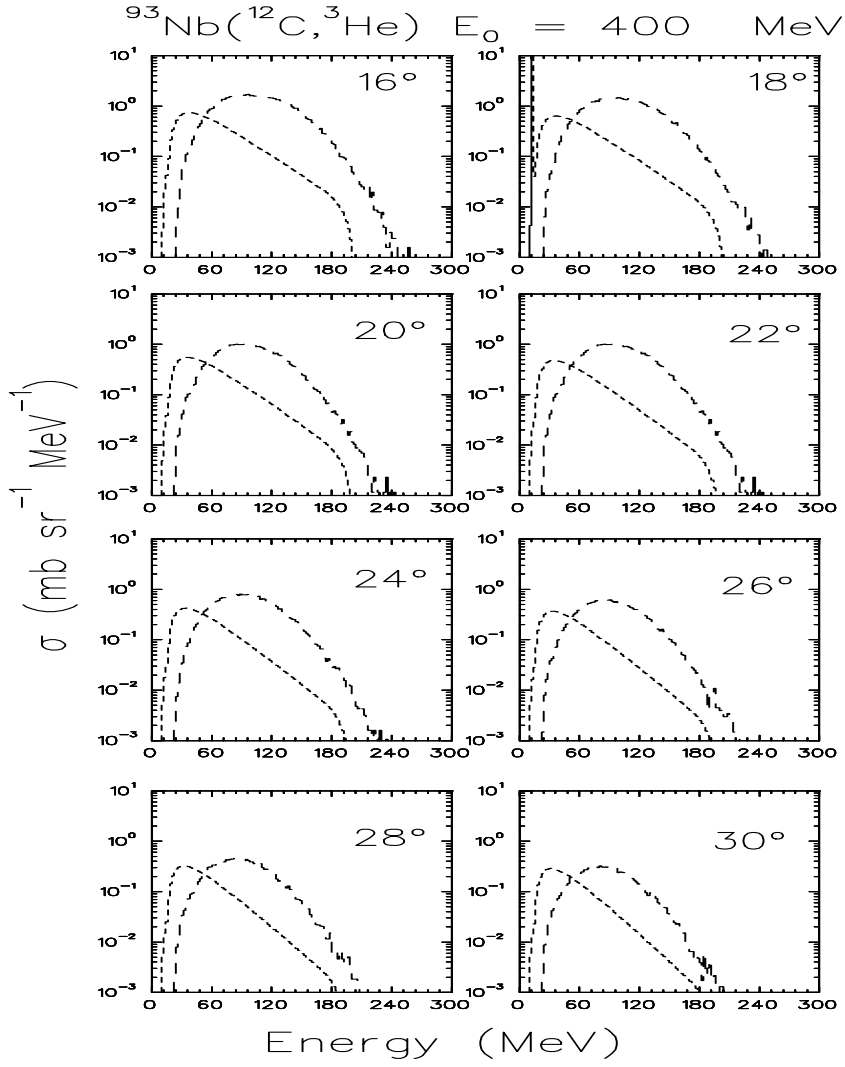

Figure 5.4: Laboratory energy spectra of ^{3}He produced in the interaction of ^{12}C with ^{93}Nb at 400 MeV. The theoretical results shown are for the break-up and coalescence contributions at the emission angles indicated. The contribution of the spectator fragment after break-up is given by the dashed lines while the contribution from coalescence is given by the dotted lines.

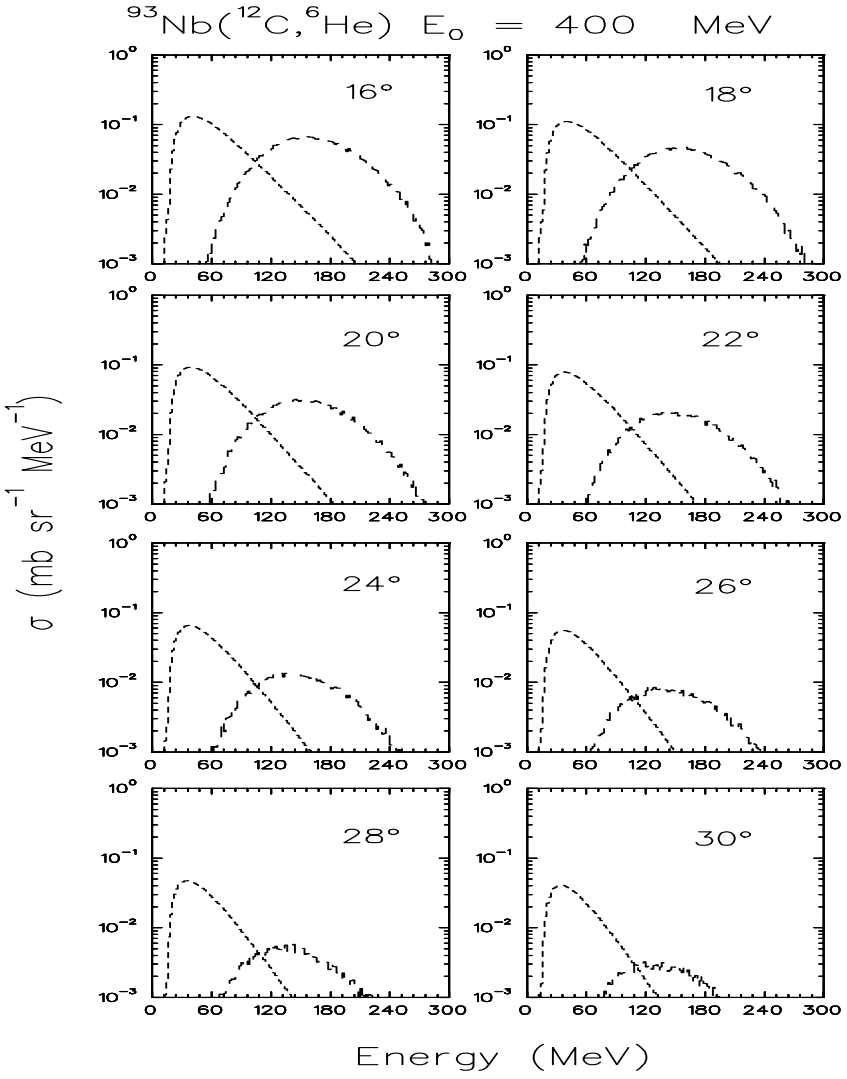

Figure 5.5: Laboratory energy spectra of ^{6}He produced in the interaction of ^{12}C with ^{93}Nb at 400 MeV. The theoretical results shown are for the break-up and coalescence contributions at the emission angles indicated. The contribution of the spectator fragment after break-up is given by the dashed lines while the contribution from coalescence is given by the dotted lines.

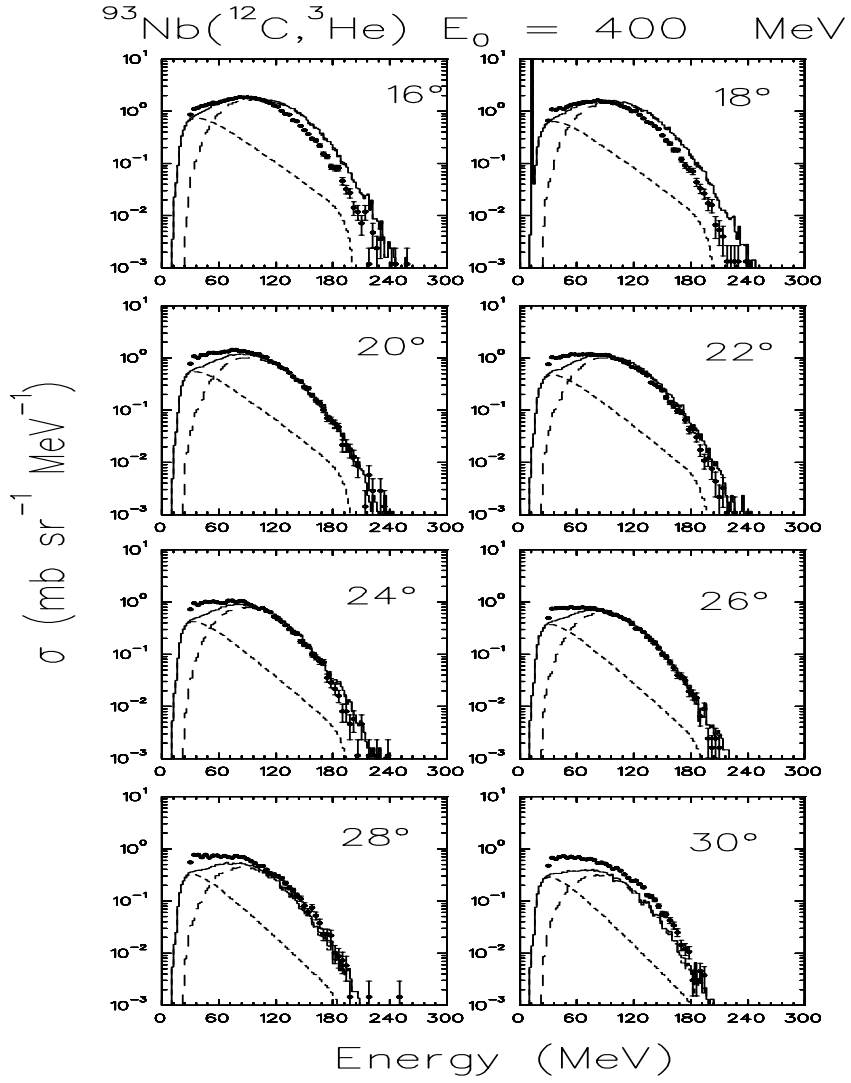

Figure 5.6: Laboratory energy spectra of ^{3}He produced in the interaction of ^{12}C with ^{93}Nb at 400 MeV. The results are shown as incoherent sum of two contributions. The measured energy spectra are indicated by the black dots. The contribution of the spectator fragment after break-up is given by the dashed lines that extend to higher emission energies while the coalescence contribution is given by the dotted lines which extend up to 180 MeV. The error bars show the statistical error.

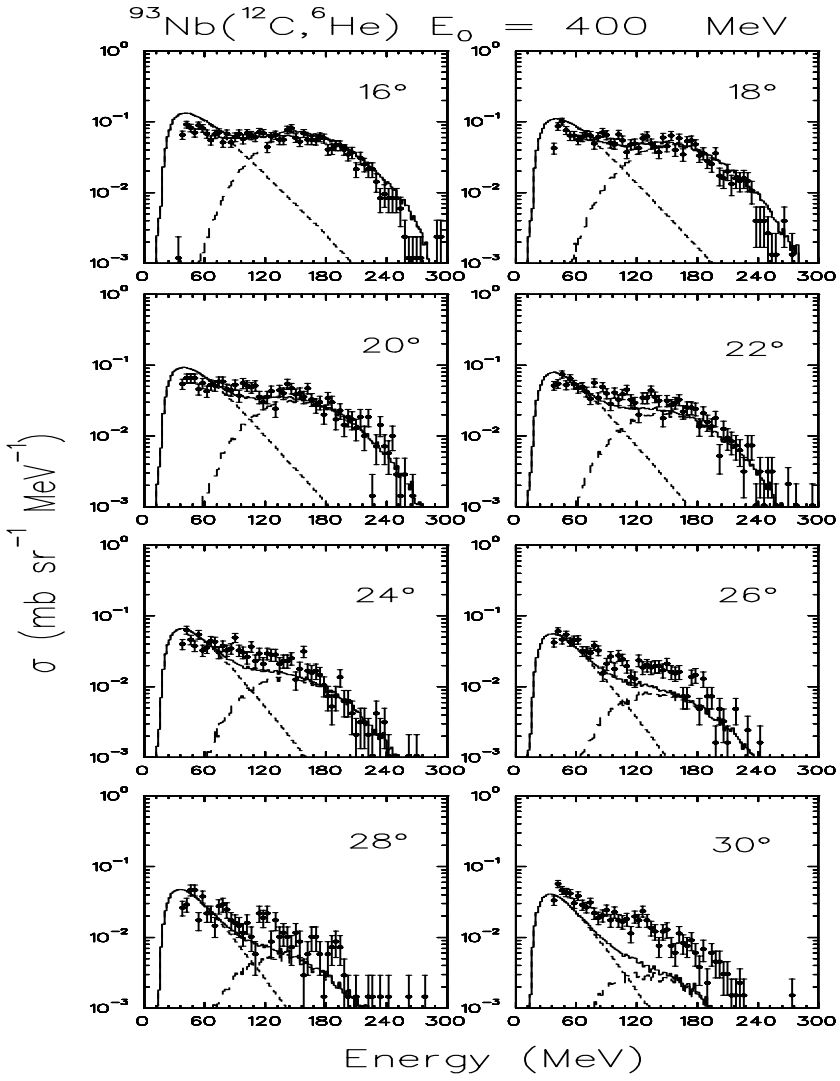

Figure 5.7: Laboratory energy spectra of ^{6}He produced in the interaction of ^{12}C with ^{93}Nb at 400 MeV. The results are shown as incoherent sum of two contributions. The measured energy spectra are indicated by the black dots. The contribution of the spectator fragment after break-up is given by the dotted lines which extend up to 200 MeV. The error bars show the statistical error.

Chapter 6

Summary and Conclusions

The present study had two aims. The first was to test the efficiencies of the detectors in telescopes 1 and 2. The second aim was to extract the double differential cross sections of ^{3}He and ^{6}He from the prescaled singles spectra of ^{3}He and ^{6}He, and explain some of the features of the spectra in terms of a theoretical model.

The efficiencies and energy calibrations of the detectors were checked by overlaying the current prescaled singles data on to existing cross sections obtained for the same reaction. In the case of the ^{3}He particles, the absolute normalization was confirmed by overlying the ^{3}He data on to the ^{3}He data from the interaction of ^{14}N with ^{93}Nb.

From the theoretical treatment of the double differential cross sections of ^{3}He and ^{6}He, it can be concluded that the spectra of these fragments can be reproduced by assuming reaction mechanisms such as projectile break-up and nucleon coalescence. These were used previously to also explain the emission of ^{4}He particles and other intermediate mass fragments emitted in the same reaction. Using the present ^{3}He and ^{6}He spectra, it was possible to refine the

theoretical model, since these fragments were not considered in the previous analyses of the ^{93}Nb(^{12}C, α) and ^{93}Nb(^{12}C, α, ^{8}Be) data. Since the theoretical approach reproduces the experimental normalized spectra satisfactorily, it can be concluded that the double differential cross sections of the emitted ^{3}He and ^{6}He fragments can to a very large extent be explained by the same reaction mechanisms as is the case for the emission of alpha particles and other intermediate mass fragments.

Upon overall interpretation of the data, the study has shown that isotope-mass separation is possible as is the case with the previous study of ^{7}Be and ^{9}Be fragments. There is a good qualitative and quantitative description of the features in the spectra of these fragments as compared to the alpha particle spectra and other intermediate mass fragments. Similar to the study of ^{7}Be and ^{9}Be fragments, a good quantitative description of ^{3}He and ^{6}He could be obtained by only taking into account the initial-state interaction between the projectile and the target nucleus. Both the earlier study of the Be isotopes and the He isotopes have shown that final state interactions are unlikely to play a significant role.

This study has again emphasized the importance of mass separation in measuring fragments of this kind. In order to separate masses of IMF's for instance, either a magnetic spectrometer or the time of flight technique could be used.

Appendix A

A.1 Overview

The input parameters that were used in the theoretical nucleon coalescence and break-up calculations are described in the following sections. The multiplicity of particles and clusters emitted during pre-equilibrium emission were evaluated using a set of coupled Boltzmann Master equations as described in chapter 4, section 4.41. The code developed at the University of Milan is HMBPZSMD17, where

- HMB stands for Harp, Miller and Berne
- PZ is the momentum along the beam axis
- SMD17 is the current version of the code

At the end of the pre-equilibrium phase, the multiplicity of unbound particles and the time evolution of the occupied states are stored into files, which are then used as inputs into the Monte Carlo code to calculate a large number of cascades during the relaxation of the compound nucleus. A phenomenological procedure by Dostrosvsky et al. [Dos59] decides if

the particle is emitted and the type of particle emitted. This procedure by [Dos59] is based on the comparison between an extracted random number and the elements of a vector giving the partial average multiplicities of the particles emitted.

A.1.1 Theoretical calculation parameters used in the coalescence contribution

In order to calculate the coalescence contribution the number of integration steps, the time length of the step, as well as the starting time of each step were modeled into the code. Also modeled into the code are the number of protons Z and number of neutrons N as well as the incident energy of the projectile. The parameter that considers the acceleration of the particles, *SLATO*, has a proportionality dependence to the increase of energy as well as the difference between the Fermi energies of the projectile or target with the fermi energy of the composite nucleus. During the fusion of the projectile with the target the value was set to 0.00. The maximum energy for the internal momentum distribution along the beam axis was set to 150 MeV, while the values for the energy steps and the momentum steps were set to 4 and 0.5, respectively. The protons and neutrons binding energies values were calculated from Kox et al. [Kox87]. The neutron inverse cross sections were taken from [Dos59] while the proton inverse cross section were taken from [Kox87].

Other parameters that were used in the code include

- ICOU, which describes the acceleration of nuclei by the Coulomb barrier. It is expressed in units of MeV.

- R_o, the interaction radius given by the expression $V_c = \frac{1}{4\pi\varepsilon_o}\frac{Z_P Z_T e^2}{R_o}$, Z_P and Z_T are the number of protons for the projectile and target nucleus, respectively, and e^2 is the electronic charge

- Q_s, the separation energy in (MeV)
- P_1 and P_2, are the momentum components expressed in (MeV/c)
- *ff*, parameter that allows the choice for the distribution function for the projectile and target nucleus
- BINBU, break-up binding energy for the particular mechanism
- Q_{REA}, fusion Q_{value} in (MeV)
- IFUN, parameter which allows for the selection of the wave function that describes the momentum distribution within the projectile
- CF and ICF, complete and incomplete fusion processes

A.1.2 Theoretical calculation parameters used in the break-up contribution

The parameters that were used to calculate the break-up contribution include the break-up Q_{value} and BINDBU. The parameters used for the emission of ^{4}He particles and other intermediate mass fragments (IMFs) are obtained from previously published data in [Gad03] [Bec03] [Gad99] and [Gad01]. The values given in this appendix are only applicable for ^{3}He and ^{6}He particles.

Table A.1: Parameters used to calculate the nucleon momentum density distribution, where ICOU = 0 MeV and R_0 = 1.63 fm

Nucleus	*ff*	P_1(MeV/c)	P_2(MeV/c)	E_f (MeV)
^{12}C	G	63	117	27.4
^{93}Nb	SW	242.5	13.25	33.45
CN	-	-	-	33.65

Table A.2: Input parameters used in the calculation for emission of ^{3}He and ^{6}He particles in the reaction ^{12}C + ^{93}Nb

Particle	V_c(MeV)	R_o (fm)	E_F(MeV/n)	$P_{c,F}$(MeV/c)
^{3}He	10.989	1.45	13.0	156
^{6}He	10.057	1.48	21.0	198

Table A.3: Input parameters used in the calculation of the break-up contribution

Process	σ(mb)	Q_{REA}(MeV)	*BINDBU*	*IFUN*	V_o(MeV)
CF	430	-	-	-	-
ICF ^{3}He	^{9}Be	-15.365	26.2788	1	100
ICF ^{6}He	^{6}Be	-19.228	35.967	5	70

Table A.4: Other input parameters used in the calculation of the break-up contribution

Process	σ(mb)	L_{min}	L_{max}	C_{bin1}(MeV)	C_{bin2}(MeV)	ΔCB(MeV)	kk'
CF	430	-	-	-	-	-	-
ICF ^{3}He	95	70	70	50	300	1	0.02
ICF ^{6}He	5	70	70	50	200	1	0.02

Bibliography

[Awe81] T. C. Awes, G. Poggi, C. K. Gelbke, B. B. Back, B. G. Glagola, H. Bruer, V. E. Viola. *Phys. Rev.* C **24**, (1981) 89

[Awe82] T. C. Awes, S. Saini, G. Poggi, C. K. Gelbke, D. Cha, R. Legrain, G. D. Westfal. *Phys. Lett.* C **25**, (1982) 2361

[Bal64] V. V. Balashov, A. N. Boyarkina, and I. Rotter. *Nucl. Phys.* **59**, (1964) 417

[Bec03] B. Becker, F. Albertini, E. Gadioli, G. F. Steyn, M. Cavinato, S. H. Connell, A. A. Cowley, E. Fabrici, S. V. Förtsch, E. Gadioli Erba, J. J. Lawrie, and E. Sideras Haddad. *Eur.Phys.* J. **18**, (2003) 639

[Ber88] G. F. Bertsch, S. Das Gupta. *Phys.Rep.* **160**, (1988) 189 and references therein

[Bru95] C. Brusati, M. Cavinato, E. Fabrici, E. Gadioli, E. Gadioli Erba. *Z. Phys.* A **353**, (1995) 57

[Cav96] M. Cavinato, E. Fabrici, E. Gadioli, E. Gadioli Erba, M. Galmarini and A. Gritti. *Z. Phys.* A **347**, (1994) 471

[Cav97] M. Cavinato, E. Fabrici, E. Gadioli Erba, and E. Risi. *Phys. Lett.* B**405**, (1997) 219

[Cav98] M. Cavinato, E. Fabrici, E. Gadioli, E. Gadioli Erba, and E. Risi. *Nucl. Phys.* A **643**, (1998) 15

[Cav01] M. Cavinato, E. Fabrici, E. Gadioli, E. Gadioli Erba, and G. Riva. *Nucl. Phys.* A **679**, (2001) 753

[Cer92] I. Cervesato, E. Fabrici, E. Gadioli, E. Gadioli Erba, and M. Galmarini. *Phys. Rev.* C **45**, (1992) 2369

[Chu94] J. L. Chuma. PHYSICA Programme. *Reference Manual*, (1994).

[Dos59] I. Dostrovsky. Z. Frankel, and G. Friedlander. *Phys. Rev.* **116**, (1959) 683

[Fuc94] H. Fuchs and K. Möhring. *Rep. Prog. Phys* **57**, (1994) 231-324

[Gad97] E. Gadioli, C. Birattari, M. Cavinato, E. Gadioli Erba, V. Allori, C. Bovati, F. Cerutti, A. Di Filipo, E. Galbiati, T. G. Stevens, S.H. Connel, J. P. F. Sellschop, S. J. Mills, F. M. Nortier, G. F. Steyn, C. MArchetta. *Phys. Lett.* B **394**, (1997) 29

[Gad98] E. Gadioli, C. Birattari, M. Cavinato, E. Fabrici, E. Gadioli Erba, V. Allori, C. Cerutti, A. Di Filipo, S. Vailati, T. G. Stevens, S. H. Connel, J. P. Sellschop, F. M. Nortier, G. F. Steyn, C. Marchetta. *Nucl. Phys.* A **641**, (1998) 271

[Gad99] E. Gadioli, M. Cavinato, E. Fabrici, E. Gadioli Erba, C. Birattari, I. Mica, S. Solia, G. F. Steyn, S. V. Förtsch, J. J. Lawrie, F. M. Nortier,T. G. Stevens, S. H. Connell, J. P. F. Sellschop, A. A. Cowley. *Nuclear Physics* A **654**, (1999) 523-540

[Gad01] E. Gadioli, G. F. Steyn, C. Birattari, S. H. Connell, A. A. Cowley, E. Fabrici, S. V. Förtsch, E. Gadioli Erba, J. J. Lawrie,

F. M. Nortier, J. P. F. Sellschop, and E. Seideras Haddad. *Eur. Phys.* J. A **11**, (2001) 161-173

[Gad03] E. Gadioli, G. F. Steyn, F. Albertini, C. Birattari, M. Cavinato, S. H. Connell, A. A. Cowley, E. Fabrici, S. V. Förtsch, E. Gadioli Erba, J. J. Lawrie, M. Pigni, J. P. F. Sellschop,and E. Seideras Haddad. *Eur. Phys.* J. A **17**, (2003) 175

[Gel77] C. K. Gelbke, D. K. Scott, M. Bini, D. C. Hendrie, J. L. Laville, J. Mahoney, M. C. Mermaz, C. Olmer. *Phys.Lett.* B **70**, (1977) 415

[Gel78] C. K. Gelbke. *Phys.Rep.***42**, (1978) 311

[Har68] G. D. Harp, J. M. Miller, B. J. Berne. *Phys. Rev.* **165**, (1968) 1166

[Hil53] J. Hill, J. A. Wheeler. *Phys. Rev.* **89**, (1953) 1102

[Hod97] P. E. Hodgson, E. Gadioli and E. Gadioli Erba. *Introductory Nuclear Physics (Oxford University Press Inc., New York*, 1997)

[Hus81] M. S. Hussein, K. W. McVoy, D. Saloner. *Phys. Lett.* B **98**, (1981) 162

[Jip84] P. Jipsen, ELOSS, *A Programm for Calculating The Ranges of Ions In Matter, National Accelerator Center* (1984)(unpublished)

[Kox87] S. Kox, A. Gamp, C. Perrin, A. Arvieux, J. Bertholet, J. F. Braundent, M. Buenerd, R. Cherkaoui, A. J. Cole, Y. E1-Masir, N. Longequeue, J. Menet, F. Merchez, and J. B. Viano. *Phys. Rev.* C **35**, (1987) 1678

[Mac88] E. W. Macdonald. *General Purpose Monte Carlo Simulation Code for Break-up Reactions, UNIMONTE, University of Edinburgh*,(1988) (unpublished)

[Mar85] F. Guzman Martinez, R. Reif. *Nucl. Phys.* A **436**, (1985) 294

[McV80] K. W. McVoy, M. Carolina Nemes. *Z. Phys.* A **295**, (1980) 177

[Mic94] K. Michaelin, A. Menchaca-Rocha, E. Belmont-Moreno. *Nuclear Instruments and Methods in Physics Research* A **356**, (1995) 297-303

[Möh91] K. Möhring, T. Srokowski, D. H. E. Gross, H. Homeyer. *Nucl. Phys.* A **533**, (1991) 333

[Ser47] R. Serber. *Phys.Rev.* **72**, (1947) 1008

[Ver93] P. Vergani, E. Gadioli, E. Vaciago, E. Fabrici, E. Gadioli Erba, and M. Galmarini. *Phys. Rev.* C **48**, (1993) 1815

[Woz92] E. W. Macdonald, A. C. Shotter, D. Branford, J. Raihigi, T. Davinson, N. J. Davis, Y. El Mohri and J. Yorkston. *Nuclear Instruments and Methods in Physics Research.* A **317**, (1992) 498-505